water

MDPI

Article

Extreme Pressures and Risk of Cavitation in Steeply Sloping Stepped Spillways of Large Dams

Jorge Matos [1,*], Carolina Kuhn Novakoski [2], Rute Ferla [3], Marcelo Giulian Marques [3], Mauricio Dai Prá [3], Alba Valéria Brandão Canellas [4] and Eder Daniel Teixeira [3]

1 CERIS, Instituto Superior Técnico, Universidade de Lisboa, 1049-001 Lisbon, Portugal
2 Coordenadoria Acadêmica, Universidade Federal de Santa Maria, Campus Cachoeira do Sul, Cachoeira do Sul 96503-205, RS, Brazil; carolina.novakoski@ufsm.br
3 Instituto de Pesquisas Hidráulicas, Universidade Federal do Rio Grande do Sul, Porto Alegre 91501-970, RS, Brazil; rute.ferla@ufrgs.br (R.F.); mmarques@iph.ufrgs.br (M.G.M.); mauricio.daipra@ufrgs.br (M.D.P.); eder.teixeira@ufrgs.br (E.D.T.)
4 Laboratório de Hidráulica Experimental e Recursos Hídricos, Furnas Centrais Elétricas S.A., Rio de Janeiro 22723-497, RJ, Brazil; alba@furnas.com.br
* Correspondence: jorge.matos@tecnico.ulisboa.pt

Abstract: Stepped spillways have been increasingly used to handle flood releases from large dams associated with hydropower plants, and it is important to evaluate the fluctuating pressure field on the steps. Hydraulic model investigations were conducted on three 53° (1V:0.75H) sloping and relatively large-stepped chutes to characterize the mean, fluctuating, and extreme pressures acting on the most critical regions of the step faces, near their outer edges. The pressure development along the chutes is presented, generally indicating an increase of the modulus of pressure coefficients up to the vicinity of the point of inception of air entrainment, and a decrease further downstream. The extreme pressure coefficients along the spillway are fitted by an empirical formula, and the critical conditions potentially leading to cavitation on prototypes are calculated. The correlation between the cavitation index and the friction factor is also applied for predicting the onset of cavitation on prototypes, and the results are compared with the pressure data-based method. Generally, the results obtained from those methods yield typical values for the cavitation index in the vicinity of the point of inception, varying approximately from 0.8 to 0.6, respectively. In light of these results, maximum unit discharges of about 15–20 m^2/s are considered advisable on 53° sloping large-stepped spillways without artificial aeration, for step heights ranging from 0.6 to 1.2 m. For much higher unit discharges, a considerable reach of the spillway may potentially be prone to the risk of cavitation damage.

Keywords: dams; stepped spillways; high-velocity flow; fluctuating pressure; extreme pressure; cavitation

Citation: Matos, J.; Novakoski, C.K.; Ferla, R.; Marques, M.G.; Dai Prá, M.; Canellas, A.V.B.; Teixeira, E.D. Extreme Pressures and Risk of Cavitation in Steeply Sloping Stepped Spillways of Large Dams. *Water* **2022**, *14*, 306. https://doi.org/10.3390/w14030306

Academic Editors: Jochen Aberle and Robert Boes

Received: 10 September 2021
Accepted: 5 January 2022
Published: 20 January 2022

1. Introduction

Flood-control structures designed to release excess water safely from a reservoir, with the aim of preventing water from spilling over the dam crest, are relevant to major hydropower schemes.

Since the 1980's, techniques such as roller compacted concrete (RCC) have greatly renewed the interest in using stepped spillways, namely on large dams. Some notable examples of prototype applications can be found elsewhere, namely in [1–3]. In particular, various stepped spillways have been incorporated in hydropower schemes, such as the Stagecoach (USA), Petit Saut (French Guayana), Dachaoshan and Shuidong (China), Pedrógão (Portugal), and Dona Francisca, Santa Clara-Jordão, and Anta dams (Brazil). Figure 1a,b illustrates the spillways of the Pedrógão and Dona Francisca dams in operation.

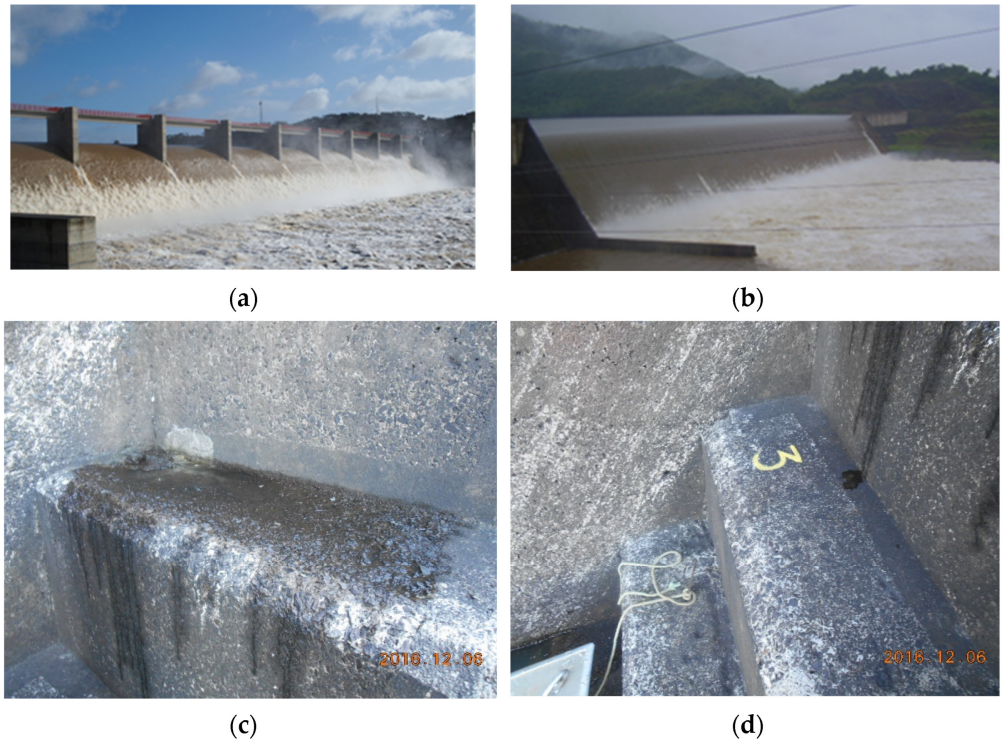

Figure 1. Pedrógão (**a**) and Dona Francisca (**b**–**d**) dam spillways: (**a**,**b**) in operation, for discharges lower than those corresponding to design conditions, in particular for Pedrógão: (**c**,**d**) some damaged steps of the Dona Francisca dam, after a major flood event in December of 2010; (**a**) courtesy Jorge Vazquez, EDIA; (**b**–**d**) courtesy Dona Francisca Energética S.A.

Initially, the unit discharge was frequently limited to some 15 m^2/s, such as on the Monskvile (USA) and De Mist Kraal (South Africa) dams, in 1986, Upper Stillwater (USA) and Les Olivettes (France) dams, in 1987, Wolwedans dam (South Africa), in 1990, and La Puebla de Cazalla dam (Spain), in 1991. Since then, larger values have been considered, such as for the Santa Clara-Jordão (unit design discharge q = 27 m^2/s), Dona Francisca (q = 32 m^2/s), Pedrógão (q = 40 m^2/s), and particularly for the Shuidong (q = 100 m^2/s) and Dachaoshan (q = 165 m^2/s) dams. It should be noted that, in Shuidong and Dachaoshan dams, the spillway configurations were unconventional. In fact, both spillways included flaring pier gates, and, on the latter, a small flip bucket at the downstream end of the piers. According to [4], the objective of such a solution was to enhance self-aeration of the flow and provide enough aeration at the pseudo-bottom (near the step faces). It was also stated by [4] that there would not be enough aeration if the design/check flood discharges of the Dachaoshan chute spillway (165 and 250 m^2/s, respectively) flowed onto the steps directly, which could possibly cause some cavitation damage.

To date, major overflow events have occurred on stepped spillways worldwide, and as far as it can be assessed, the performance of stepped spillways on RCC or concrete gravity dams has been satisfactory [2,5,6]. However, on the Dona Francisca dam, some steps presented localized damage after a major flood event in December of 2010 [7]. According to records provided by the Dona Francisca Energética S.A. company, the unit discharge was above 20 m^2/s and 15 m^2/s for approximately seven and fourteen hours, respectively. In light of the analysis presented in Section 4, the occurrence of cavitation would seem possible for flows of this magnitude on such a type of stepped spillway. It should be noted, however, that on the D. Francisca dam the steps are chamfered, so the previous observation should be carefully interpreted. At Paradise dam, no damage to the stepped chute itself was reported after a succession of major flood events that took place between 2010 and 2013 [6]. In turn, damages were recorded at the basin apron, with pronounced downstream scouring [8,9].

Among the aspects of relevance for the hydraulic design of stepped spillways, the pressure field acting on the step faces has been the subject of in-depth investigation. In [10–12], mean pressures were acquired on the step faces, whereas mean, fluctuating, and extreme pressures were obtained in other studies, such as [13–32]. The doctoral dissertations of [17,21,27], in particular, addressed the fluctuating pressure field on the horizontal and vertical step faces of steeply sloping stepped spillways with uncontrolled ogee crests, typical of RCC or concrete gravity dams. Therein, the external region of the horizontal tread, located near the step edge, was found to be influenced by the main stream, whereas the internal part, located around the inner corner, was mainly influenced by the recirculating vortices. Those studies also revealed that the maximum pressure is located on the external region of the horizontal face of the steps, due to the impact of the main flow, whereas the minimum pressure occurs near the outer edge of the vertical face, due to the drag effect caused by the main stream [18]. Empirical models have been developed for predicting the mean and fluctuating pressure distributions along the vertical and horizontal step faces [19,20], or the development of the mean, fluctuating, and extreme pressure coefficients down the chute [21,22,27,29]. Based on the extreme pressures near the outer edge of the vertical face of the steps with 0.1% probability of non-exceedance, cavitation risk was estimated in [21,22,27,32]. In turn, [33] conducted experiments of high velocity flow in a closed conduit, using acoustic emission technology for detecting cavitation characteristics along with high-speed videography, providing additional insight into the flow features that drive the formation of cavitation. The critical cavitation index represented the point of the largest increase in the rate of cavitation activity, a point where performance could be affected. The correlation between the critical cavitation index and the friction factor proposed by [34] for uniformly distributed roughnesses in turbulent boundary layers was found to be applicable in skimming flows. This correlation was applied by [2,35] for predicting the onset of cavitation at the point of inception of skimming flow on 1V:0.75H steeply sloping stepped spillways.

The objective of this study was, firstly, to extend the set of data gathered in previous studies by increasing the maximum unit discharge and the critical flow depth normalized by the step height. Further, by acquiring an extensive set of simultaneous pressure measurements near the outer edges of the vertical and horizontal faces of the steps, embracing the non-aerated and self-aerated flow regions, the aim was to develop robust empirical models for estimating the extreme pressures down the chute. Another goal of the present study was to perform a comparative analysis of the conditions leading to the onset of cavitation and the extension of the spillway potentially prone to cavitation damage, based on the findings of [33], against those derived from the analysis of extreme (minimum) pressures near the outer edge of the vertical face of the steps.

2. Materials and Methods

The experiments were carried out in the framework of [32]. Three relatively large experimental facilities were assembled, two of which (LOH I and LOH II) at the Laboratory of Hydraulic Works of the Institute of Hydraulic Research, Federal University of Rio Grande do Sul (IPH-UFRGS), and the third one at the Laboratory of Experimental Hydraulics (LAHE) of Furnas Centrais Elétricas, also in Brazil.

The stepped spillway physical models used in this research included steps made of metal (LOH I, LOH II) and smooth concrete (LAHE) (Figure 2). The height of the stepped chutes, from crest to toe (H) was 2.45 m (LOH I), 4.60 m (LOH II) and 2.30 m (LAHE), and the respective width (W) was 0.40 m (LOH I), 0.50 m (LOH II) and 1.15 m (LAHE). All stepped chutes had a pseudo-bottom angle from the horizontal $\theta = 53.13°$ (i.e., chute slope of 1V:0.75H), with a step height (h) of 0.06 m (LOH I, LOH II) or 0.09 m (LAHE) (Table 1). In all models, the uncontrolled spillway crest shapes followed the standard Waterways Experiment Station (WES) developed by the U.S. Army Corps of Engineers. Steps of variable height were not incorporated into the WES profiles. Further information can be found in [32].

(**a**) (**b**) (**c**)

Figure 2. Experimental facilities with spillway models in operation: (**a**) LOH I ($q = 0.10\ m^2/s$, $d_c/h = 1.68$, $Re = 10^5$); (**b**) LOH II ($q = 0.30\ m^2/s$, $d_c/h = 3.49$, $Re = 3.0 \times 10^5$); (**c**) LAHE ($q = 0.36\ m^2/s$, $d_c/h = 2.61$, $Re = 3.6 \times 10^5$).

Table 1. Details of the spillway models and location of the pressure taps on the step faces.

Setup	H (m)	W (m)	h (m)	l (m)	N_{TH} (−)	N_{TV} (−)	y (mm)	z (mm)	y/l (−)	z/h (−)
LOH I	2.45	0.40	0.06	0.0450	27	27	4.0	5.0	0.089	0.083
LOH II	4.60	0.50	0.06	0.0450	26	23	8.0	8.0	0.178	0.133
LAHE	2.30	1.15	0.09	0.0675	9	9	5.6	7.5	0.083	0.083

Note: H—height of the chute, from crest to toe; W—chute width; h—step height; l—step length; N_{TH}—number of pressure taps near the outer edge of the horizontal step faces; N_{TV}—number of pressure taps near the outer edge of the vertical step faces; y—distance from the external edge to the pressure tap, along the horizontal face of the step; z—distance from the external edge to the pressure tap, along the vertical face of the step (sketch in Figure 3).

Various piezoresistive sensors (Omega PX419, Sitron SP96, and Hytronic TM25, Porto Alegre, Brazil) were used to measure the pressure fluctuations on the step faces with pressure ranges from −0.05 to +0.31 bar (LOH I), −0.35 to +0.35 bar (LOH II), and −0.10 to +0.30 bar (LAHE), with accuracies ranging from 0.08% to ±0.5% FS. The pressure sensors were connected to the taps by means of 0.20-m long, 1.7-mm internal diameter silicone tubes (LOH I, LOH II), and 0.05-m long, 3.95-mm internal diameter copper tubes together with 0.20-m long, 6.35-mm internal diameter silicone tubes (LAHE). The length of the tubes met the recommendations of [36]. The notation used by [17,22] was adopted to define the measuring points (see Figure 3). The fluctuating pressures were acquired at an acquisition rate of 100 Hz, and the acquisition time was set equal to 10 min (60,000 samples per test). The selection of the sampling frequency and time was based on preliminary tests [27,30,32], being of a similar order of magnitude to those adopted by [21,22]. The location of the pressure taps is detailed in Table 1. These correspond to locations nearby those where extreme pressures would be expected, according to the findings of [19,20,22,26,27], among others.

In all models, the discharge was supplied from closed circuits with constant head reservoirs upstream of the chute, after reaching the steady state, and measured by electromagnetic flow meters installed in the supply conduits, with an accuracy of 0.25%. The unit discharges (q) tested ranged from 0.10 to 0.35 m^2/s (LOH I), 0.05 to 0.50 m^2/s (LOH II) and 0.10 to 0.36 m^2/s (LAHE), and the corresponding critical depth normalized by the step height (d_c/h, where $d_c = (q^2/g)^{1/3}$, g being the gravitational acceleration) varied

between 1.68 to 3.87 (LOH I), 1.11 to 4.90 (LOH II) and 1.12 to 2.61 (LAHE). Further details of the test program, including the Reynolds number ($Re = q/\upsilon$), along with the Froude ($Fr_i = U_i/(gd_i)^{1/2}$) and Weber ($We_i = U_i/(\sigma_w/(\rho L_s))^{1/2}$) numbers at the point of inception of air entrainment, are included in Table 2. In the above formulae, υ is the kinematic viscosity of water, U_i and d_i are the mean water velocity and equivalent clear water depth at the point of inception of air entrainment, respectively, σ_w is the surface tension between air and water, ρ is the density of water, and L_s is the distance between the step edges ($L_s = h/\sin\theta$).

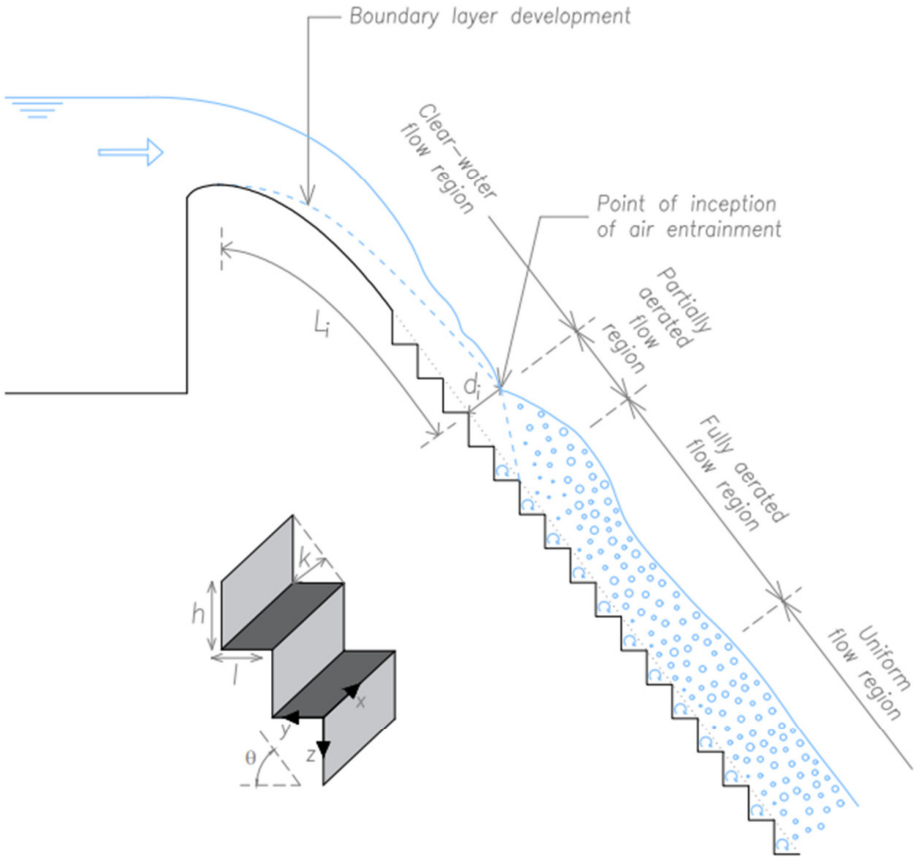

Figure 3. Sketch of the skimming flow on a steeply sloping stepped spillway and notation adopted to define the location of the pressure taps, as per [17–22].

Table 2. Test program.

Setup	q (m^2/s)	d_c/h (-)	Re (-)	Fr_i (-)	We_i (-)
LOH I	0.100	1.68	9.9×10^4	5.22	97
	0.125	1.95	1.2×10^5	5.36	105
	0.150	2.20	1.5×10^5	5.47	115
	0.200	2.66	2.0×10^5	5.66	128
	0.250	3.09	2.5×10^5	5.80	141
	0.275	3.29	2.7×10^5	5.87	147
	0.330	3.72	3.3×10^5	5.99	158
	0.350	3.87	3.5×10^5	6.03	163

Table 2. *Cont.*

Setup	q (m^2/s)	d_c/h (-)	Re (-)	Fr_i (-)	We_i (-)
LOH II	0.054	1.11	5.3×10^4	4.87	75
	0.082	1.47	8.1×10^4	5.11	91
	0.108	1.77	1.1×10^5	5.27	102
	0.150	2.20	1.5×10^5	5.47	115
	0.200	2.66	2.0×10^5	5.66	128
	0.300	3.49	3.0×10^5	5.93	153
	0.400	4.23	4.0×10^5	6.13	171
	0.500	4.90	5.0×10^5	6.29	186
LAHE	0.100	1.12	9.9×10^4	4.87	112
	0.125	1.30	1.2×10^5	5.00	126
	0.150	1.47	1.5×10^5	5.10	134
	0.200	1.78	2.0×10^5	5.28	151
	0.275	2.19	2.7×10^5	5.47	171
	0.330	2.48	3.3×10^5	5.59	185
	0.356	2.61	3.5×10^5	5.64	189

Note: q—unit discharge; d_c/h—relative critical depth, with $d_c = (q^2/g)^{1/3}$; Re—Reynolds number ($Re = q/\upsilon$); Fr_i—Froude number at the point of inception ($Fr_i = U_i/(gh_i)^{1/2}$); We_i—Weber number at the point of inception, given as $We_i = U_i/(\sigma_w/(\rho L_s))^{1/2}$.

Considering that both Fr and We increase downstream of the point of inception, practically all of the tested range of Re and We are expected to be exempted from major scale effects with regard to the main macro flow properties, such as air concentration and velocity, characteristic flow depths, and fluctuating pressures on the step faces. According to [11,37], scale effects with respect to the air concentration and velocity were negligible for $Re > 3 \times 10^4$, whereas [38,39] recommended $Re > 10^5$ and $We > 100$. A more conservative criterion was indicated by [40] for scale effects mitigation based on local air concentration close to smooth chute inverts ($Re > 2 \times 10^5$). With respect to pressures on the step faces, [21] suggested that scale effects may be neglected for $Re > 10^5$.

3. Skimming Flow on Steep Slopes: Main Regions and Flow Properties

Skimming flow down stepped spillways can be divided into various regions. In the non-aerated flow region close to the spillway crest, the boundary layer grows from the spillway floor. Outside the boundary layer the water surface is initially smooth and glassy, but it becomes undulated upstream of the inception of air entrainment. This undulated surface is responsible for the transport of air between the irregular waves, as shown elsewhere [41,42]. When the boundary layer approaches the free-surface, entrainment of air by the multitude of vortices in the turbulent flow begins at the so-called point of inception [1,43,44]. Self-entrainment into the step niches occurs in the vicinity of the point of inception as a consequence of recurring significant surface troughs combined with bubbly flow protruding to the steps [45]. As a result of the highly macroroughness induced turbulence, a rapidly varied air-water flow takes place in a short region further downstream, in contrast with the traditional concept of gradually varied self-aerated flow on smooth chutes [2,41,46]. The location of the section separating the rapidly from the gradually varied flow region was found to occur for $L' \sim 30$, irrespective of the relative critical depth [2,41,47]. The normalized distance $L' = (L - L_i)/d_i$, where L is the streamwise distance from the crest to the outer edge of the step, d the equivalent clear water depth, and the subscript i refers to the point of inception (Figure 3).

Downstream of the rapidly varied flow region, a trend of a slight increase in the mean air concentration and flow bulking is noticeable along the chute, with a wavy pattern [2,41]. From a practical standpoint, the waviness may be considered negligible, and the flow will become virtually quasi-uniform far downstream of the point of inception. Then, for a given discharge, the main flow properties, such as the mean air concentration, equivalent clear water depth, mean water velocity, and mean pressure distribution on the steps, will practically not vary along the spillway.

Various formulae have been proposed for estimating the location and flow properties at the point of inception in steeply sloping stepped chutes, typical of RCC dams, as well as the main flow properties upstream and downstream of that location, such as [6,39,41,42,44,48–50]. Herein, the formulae developed based on the experimental work gathered on a 1V:0.75H sloping chute [51–53] were adopted. These include:

Location and equivalent clear water depth at the point of inception [42]:

$$\frac{L_i}{k} = 6.75\, F_*^{0.76} \quad (1)$$

$$\frac{d_i}{k} = 0.35\, F_*^{0.59} \quad (2)$$

where k is the step roughness height ($k = h\cos\theta$) and F_* is a Froude number defined as $F_* = q/(g \sin\theta\, k^3)^{1/2}$.

Equivalent clear water depth, upstream of the point of inception [42]:

$$\frac{d}{d_i} = 1.17 - 0.25\frac{L}{L_i} + \frac{0.084}{L/L_i} \quad (3)$$

Equivalent clear water depth, downstream of the point of inception [41,47]:

$$\frac{d}{d_i} = \frac{1}{\left\{1 + \left[21.338 - \frac{13.815}{(d_c/h)^2}\right]^{-1} L'^{1/2}\right\}} \quad (4)$$

$$\frac{d}{d_i} = 0.653 + 0.347\, e^{-\frac{L'}{27.60}} \quad (5)$$

where $L' = (L - L_i)/d_i$. Equation (4) was applied for $d_c/h \leq 3$, whereas Equation (5) was adopted for $d_c/h > 3$.

The mean water velocity is given as $U = q/d$.

Air concentration close to the pseudo-bottom, downstream of the point of inception [50,51]:

$$C_b = \frac{0.381}{1 + \left(\frac{L'}{14.189}\right)^{-1.232}} \quad (6)$$

where C_b was obtained at a distance of 0.32 cm from the pseudo-bottom, along its normal.

4. Results and Application

4.1. Pressure Development and Duration of Negative Pressures

In order to evaluate the development of mean and fluctuating pressure along the chute near the outer edges of the horizontal and vertical step faces, the following parameters were analyzed: (1) mean (time-averaged) pressure p_m; (2) root mean square value representative of the pressure fluctuations p'; and (3) extreme pressures characterized by $p_{x\%}$, x% being the probability of non-exceedance, that is, the probability of occurrence of lower pressure values. Herein, the limits 0.1%, 1.0%, and 5.0% were chosen for the minimum pressures, whereas 95.0%, 99.0%, or 99.9% were adopted for the maximum pressures, in accordance with other studies [18,19,22,27]. These parameters were derived from the pressure measurements

acquired simultaneously on the vertical and horizontal faces of the steps, at a frequency of 100 Hz.

Figure 4 shows the streamwise development of the dimensionless mean, fluctuating, and extreme pressures at the LOH II stepped chute, near the outer edges of the vertical and horizontal step faces, for two relative critical depths. Also included in the same figure is the location of the point of inception, based on Equation (1).

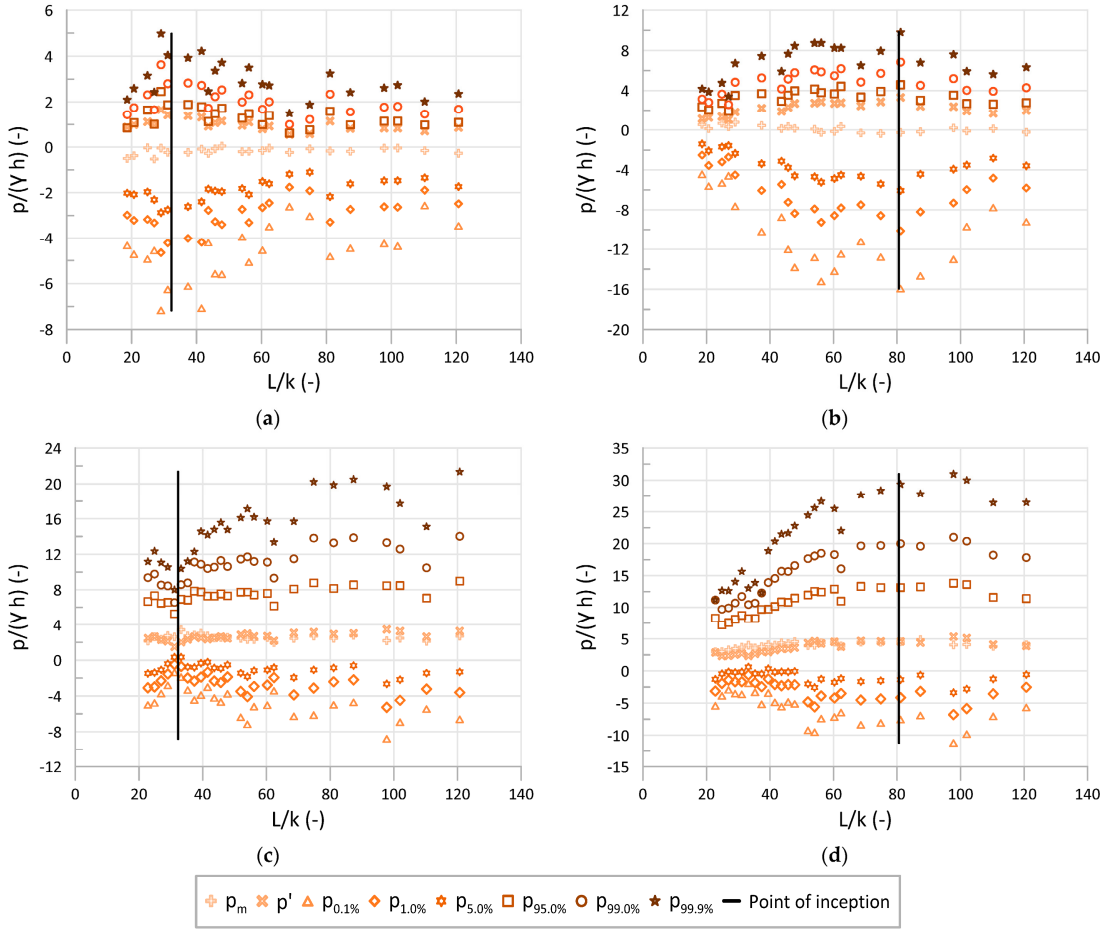

Figure 4. Streamwise development of the dimensionless mean, fluctuating, and extreme pressures at the LOH II stepped chute: (**a**) vertical face of the step, near the outer edge ($z/h = 0.133$), for $d_c/h = 2.20$; (**b**) vertical face of the step, near the outer edge ($z/h = 0.133$), for $d_c/h = 4.90$; (**c**) horizontal face of the step, near the outer edge ($y/l = 0.178$), for $d_c/h = 2.20$; (**d**) horizontal face of the step, near the outer edge ($y/l = 0.178$), for $d_c/h = 4.90$.

The following conclusions may be drawn (also generally valid for the LOH I and LAHE stepped chutes, not shown herein). Near the outer edge of the vertical step faces, the mean pressure is slightly negative or almost null, for both discharges (Figure 4a,b); the fluctuating (p') and extreme pressures $p_{95.0\%}$, $p_{99.0\%}$, $p_{99.9\%}$ tend to increase upstream of the point of inception, whereas the extreme pressures $p_{5.0\%}$, $p_{1.0\%}$, $p_{0.1\%}$ tend to decrease (or, in alternative, their respective moduli increase). A decrease in p', $p_{95.0\%}$, $p_{99.0\%}$, $p_{99.9\%}$ (or increase in $p_{5.0\%}$, $p_{1.0\%}$, $p_{0.1\%}$), is noticeable in an initial reach downstream of that location; further downstream, the pressures tend to stabilize, while keeping a typical wavy pattern. Significant negative pressures may occur for $p_{0.1\%}$, upstream of the point of inception, particularly in its vicinity, reaching $-16\ \gamma h$, for $d_c/h = 4.90$ (Figure 4b). This corresponds to conditions that could lead (or almost) to cavitation in prototype, for step heights of 0.9 m and 0.6 m, respectively. In turn, near the outer edges of the horizontal step faces, the mean pressure is positive due to the impact of the flow, being of the order of magnitude of the

pressure fluctuations; the tendency of the fluctuating and extreme pressures to increase (in modulus) upstream of the point of inception, similar to that observed on the vertical face, is seen for the largest discharge ($d_c/h = 4.90$), namely for the positive pressures (Figure 4d); shortly downstream of that location, a slightly decreasing trend (in modulus) seem to take place. These results are partially in agreement with those reported by [18], on a similar chute slope (1V:0.8H), along the center of symmetry of the horizontal step faces, relative to p_m, p', $p_{5.0\%}$, and $p_{95.0\%}$. There, it was observed that the mean pressures were positive all along the spillway, and only minimum pressures ($p_{5.0\%}$) exhibited negative values. It was also found by [18] that both maximum and minimum pressures were located upstream of the point of inception, including for $d_c/h = 2.25$, which concurs with the results obtained herein for the vertical face of the step, but is apparently in contrast with those gathered on the horizontal face, for a similar relative critical depth ($d_c/h = 2.20$). However, the definition of the point of inception adopted by [18] was that corresponding to fully aerated flow by visual observation, which is distinct to that used herein. In fact, the point of inception was located at $L/k \sim 40$ in [18], whereas $L/k \sim 33$ was obtained in the present study. It is also important to note the distinct location of the pressure taps in both studies (i.e., in the center of the horizontal face versus near the outer step edge), so a direct comparison cannot be made. It is also interesting that significant negative pressures may likewise occur near the outer edge of the horizontal face of the steps, particularly for large unit discharges, where $p_{0.1\%}$ may reach $-10\ \gamma h$ (Figure 4d).

Figure 5 shows the streamwise development of the dimensionless mean and fluctuating pressures at the LOH II stepped chute, near the outer edges of the vertical and horizontal step faces, for various relative critical depths. Similar to what was observed by [18] at the center of symmetry of the horizontal face of the steps, a steady wavy pattern is observed down the chute, generally with so-called phase coincidence, i.e., coincidence of local maximum (peak) and minimum (valley) when considering different discharges. Near the outer edge of the vertical face of the steps, the mean pressure oscillates around zero regardless of the relative critical depth, with $p_m/(\gamma h)$ ranging approximately between ± 0.25 m for $L/k > 70$, in the gradually varied flow region. Considerable pressure fluctuations were obtained near the outer edges of the vertical and horizontal step faces, with higher magnitudes on the latter. In general, both the mean pressures and the pressure fluctuations tend to increase with the relative critical depth, as also shown in [18], when considering a similar range of d_c/h values (i.e., 1.41, 1.85 and 2.25). In the present study, the relative differences of p_m and p' are generally smaller for the largest d_c/h values (3.49 and 4.90).

The percentage of total negative pressure duration with respect to the total time of data acquisition was also investigated herein. Figure 6 presents the streamwise development of the percentage of total time during which the taps located near the outer edges of the vertical and horizontal step faces of the LOH II chute exhibit negative pressures. The results are qualitatively similar to those obtained on the LOH I and LAHE chutes (not shown herein), showing a considerable oscillation down the chute and data scatter, as would be expected, taking into account the broad range of d_c/h values. A slight increasing trend occurs in an initial reach of the spillway (e.g., $L' < 20$–40), whereas a plateau seems to occur further downstream. Near the outer edge of the vertical step faces, the percentage of total time during which negative pressures occur is significant, varying from 45 to 80%, for $L' > 40$. These values are of the same order of magnitude as those reported by [20] (~50 to 80%), for comparable relative locations of the pressure taps and a comparable range of relative critical depths (i.e., $z/h < 0.15$ and $1.42 \leq d_c/h \leq 2.25$). Near the outer edge of the horizontal step faces, the percentage of total time during which negative pressures occur is much smaller, generally ranging from 0 to 20%, and from 10 to 20% for $L' > 40$. Even though [20] obtained values up to 20% on the horizontal step faces, considerably smaller values were plotted therein (<5%) for comparable relative locations of the pressure taps. However, it should be noticed that only two locations were selected in [20] ($L/k = 69.6$ and

L/k = 63.5), whereas a broader extension of the chute was analyzed herein (approximately $-25 < L' < 160$, or $-20 < L/k < 120$).

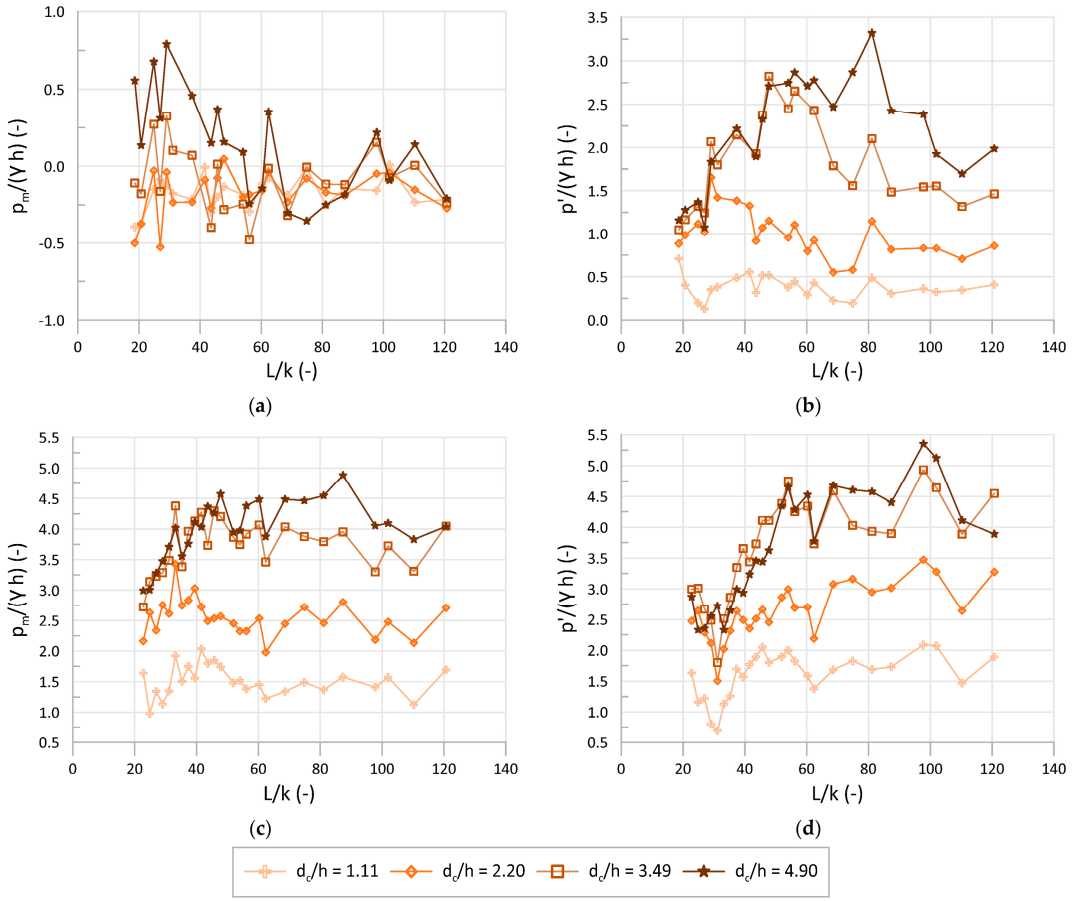

Figure 5. Streamwise development of the dimensionless mean (left) and fluctuating (right) pressures at the LOH II stepped chute: (**a**,**b**) vertical face of the step, near the outer edge (z/h = 0.133); (**c**,**d**) horizontal face of the step, near the outer edge (y/l = 0.178).

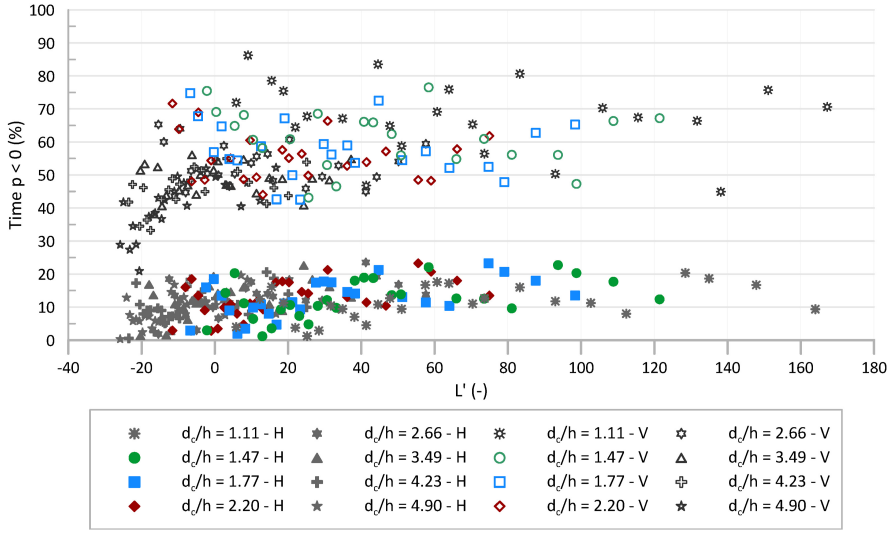

Figure 6. Streamwise development of the percentage of total time during which the taps located near the outer edge of the vertical face of the steps (z/h = 0.133, unfilled symbols) or near the outer edge of the horizontal face of the steps (y/l = 0.178, filled symbols) exhibit negative pressures. Data for the LOH II stepped chute.

4.2. Mean and Fluctuating Pressures

The mean and fluctuating pressure coefficients are defined as [21,22,28,29] $C_p = (p_m/\gamma)/(U^2/2g)$ and $C'_p = (p'/\gamma)/(U^2/2g)$, respectively. The mean water velocity at each cross section in the non-aerated region was determined from $U = q/d$, by applying Equation (3), along with Equations (1) and (2), for estimating the equivalent clear water depth; in the self-aerated region, Equations (4) and (5) were used for estimating d, for $d_c/h \leq 3$ and for $d_c/h > 3$, respectively.

Figure 7 shows the development of C_p and C'_p along the LOH II stepped chute for the pressure taps near the outer edge of the vertical and horizontal step faces, for various relative critical depths. Near the outer edge of both step faces, the mean and the fluctuating pressure coefficients exhibit distinct behaviors upstream and downstream of the point of inception, similarly to what was noted by [21,22,28]. Near the outer edge of the vertical step face, C_p is generally very small, with a decreasing trend (or increasing, in modulus) for $L' < 0$, whereas an increasing trend (or decreasing, in modulus) occurs in a short reach immediately downstream of the point of inception (Figure 7a). For L' greater than 20–40, C_p tends to stabilize around a slightly negative value, ranging between 0 and −0.02. The data presents some scatter, which may be explained by the broad range of values of the relative critical depth ($1.11 \leq d_c/h \leq 4.90$). Overall, the influence of d_c/h on C_p is not significant, except for small to moderate relative critical depths, in the vicinity of the point of inception. In turn, C'_p shows a markedly increasing trend for $L' < 0$, reaching a peak in the vicinity of the point of inception (Figure 7b); a significant decreasing trend occurs in a short reach immediately downstream of that location, followed by a milder decreasing trend for $L' > 20$–40, stabilizing around 0.02. Similarly, as observed for C_p, C'_p is not significantly influenced by d_c/h. In relation to the outer edge of the horizontal face of the steps (Figure 7c,d), both C_p and C'_p display an increasing trend upstream of the point of inception, followed by a decreasing trend downstream of that location, steeply in an initial reach, and more gently further downstream (i.e., approximately $L' > 30$). As noted by [22], the presence of air has a cushion effect, reducing the magnitude of the pressures on the step faces. Furthermore, a similar order of magnitude was obtained for C_p and C'_p on the horizontal faces of the steps, which is in line with the results presented by [22].

Interestingly, the separation between these rapidly and gradually varied flow regions downstream of the point of inception seem to occur at a location nearby that previously observed for other flow properties, such as the mean air concentration [41,51].

Figure 8 shows the development of C_p and C'_p along the stepped chutes, using the complete data sets of all facilities (Tables 1 and 2). The empirical formulae proposed by [22,27] are also plotted in Figure 8. Dashed lines were drawn herein when extending the range of application of the models developed by [22,27], or for the model developed within the scope of this study. A considerable data scatter is noticeable, due to the broad range of values of the relative critical depth (Table 2), as well as due to slightly distinct positions of the pressure taps on the horizontal and vertical faces of the steps (namely for LOH II versus LOH I and LAHE, as indicated in Table 1). These may explain the larger data scatter or slightly lower absolute values of C_p and C'_p for the LOH II model.

The model proposed by [27] generally concurs with the experimental data on indicating increasing or decreasing trends of C_p and C'_p, except for C_p on the vertical face, downstream of the point if inception. However, such a model tends to overestimate C_p and C'_p on the horizontal face of the step upstream of the point of inception (Figure 8c,d). In turn, the model of [22] provides a good qualitative representation of the overall decreasing trend of C_p on the horizontal face, for $L' < 60$ (Figure 8c), as well as that of C'_p on both faces of the steps (Figure 8b,d). Considering the significant data scatter, it was not possible to obtain an adequate model that fits all C_p and C'_p results reasonably well, except for C'_p near the outer edge of the vertical step faces (i.e., Equation (7), for $25 \leq L' \leq 50$, along with Table 3, and $C'_p \sim 0.03$, for $L' > 50$).

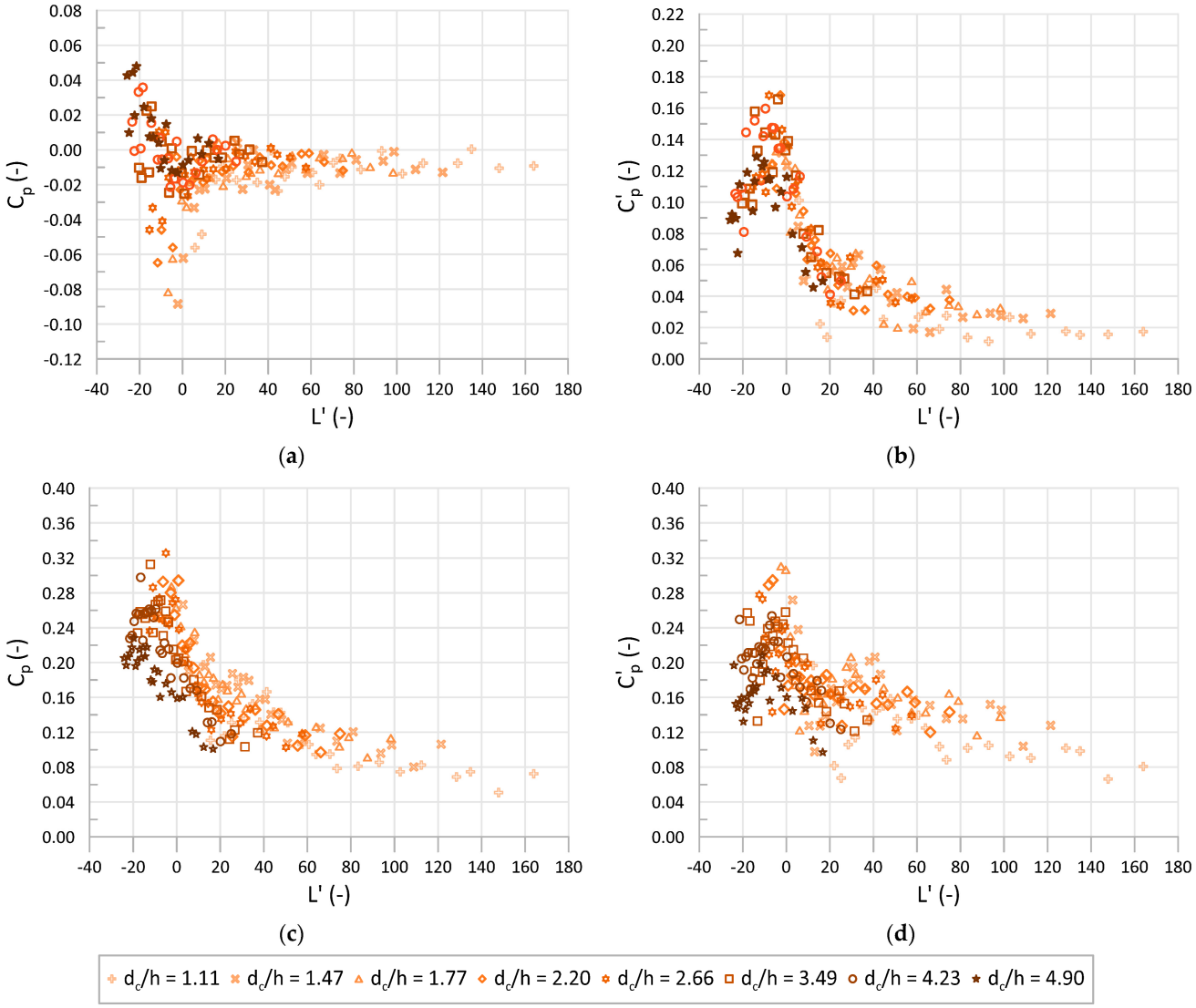

Figure 7. Streamwise development of the mean (left) and fluctuating (right) pressure coefficients, at the LOH II stepped chute: (**a**,**b**) vertical face of the step, near the outer edge (z/h = 0.133); (**c**,**d**) horizontal face of the step, near the outer edge (y/l = 0.178).

Table 3. Coefficients of Equation (7) relative to the outer edge of the vertical and horizontal faces of the steps.

Data		a	b	c	d	R^2
Full data set (vertical face) $-25 \leq L' \leq 50$	C'_p	0.1313	0.0018	0.0410	0.0020	0.80
	$C_{p0.1\%}$	−0.6507	−0.0094	0.0421	0.0024	0.80
	$C_{p1.0\%}$	−0.4210	−0.0072	0.0440	0.0024	0.79
	$C_{p5.0\%}$	−0.2626	−0.0054	0.0459	0.0023	0.76
$Re \geq 2 \times 10^5$; $d_c/h \geq 1.78$ (horizontal face) $0 \leq L' \leq 50$	$C_{p99.9\%}$	1.1759	0.0084	0.0304	−0.0003	0.46
	$C_{p99.0\%}$	0.8956	−0.0012	0.0232	−0.0003	0.58
	$C_{p95.0\%}$	0.6469	−0.0040	0.0202	−0.0003	0.62

Notes: R^2—coefficient of determination. On the horizontal face of the step, Equation (7) essentially provides an indication of the general trend of the pressure coefficient downstream of the point of inception, given the relatively low values of R^2.

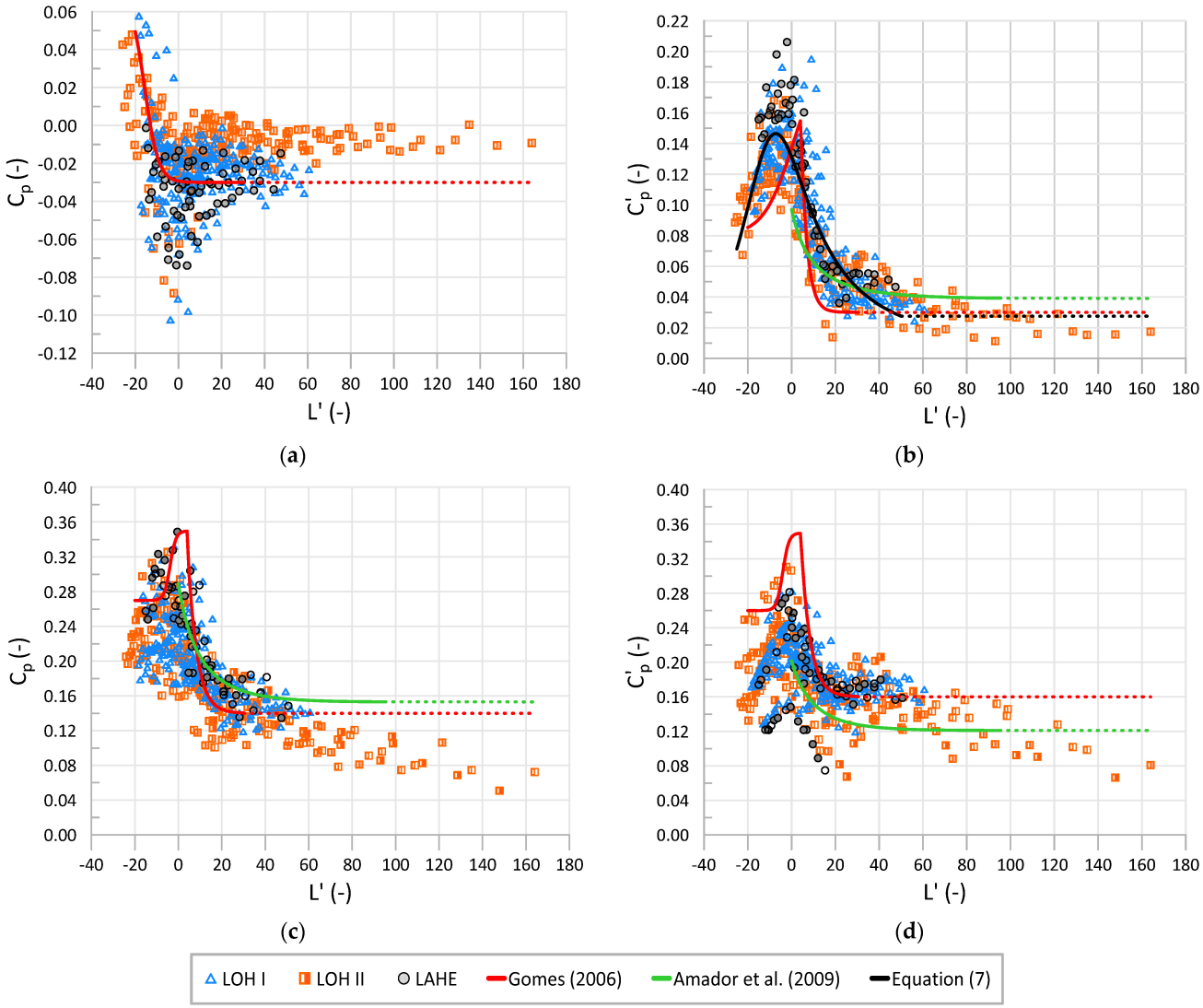

Figure 8. Streamwise development of the mean (**left**) and fluctuating (**right**) pressure coefficients, at the LOH I, LOH II, and LAHE stepped chutes: (**a**,**b**) vertical face of the step, near the outer edge; (**c**,**d**) horizontal face of the step, near the outer edge.

4.3. Extreme Pressures

The extreme pressure coefficients are defined as $C_{px\%} = (p_{x\%}/\gamma)/(U^2/2g)$ [21,22,28], where x% is the probability of non-exceedance. The limits 5.0%, 1.0%, 0.1%, and 95.0%, 99.0%, 99.9% were selected for the minimum and maximum pressures, respectively.

Figure 9 shows the development of the most extreme pressures along the LOH I, LOH II, and LAHE stepped chutes, namely, $C_{p0.1\%}$ near the outer edge of the vertical face of the steps, and $C_{p99.9\%}$ near the outer edge of the horizontal face of the steps. Overall, the observed data trends for the distinct stepped chutes are consistent. The influence of the relative critical depth is relatively small on the vertical faces. In turn, the influence of d_c/h is not as negligible on the horizontal faces, taking into account the data scatter. Similarly, as observed for C_p, there is a sharp decreasing trend (increasing in modulus) of $C_{p0.1\%}$ for $L' < 0$, whereas an increasing trend (decreasing in modulus) occurs in a short reach immediately downstream of that location (Figure 9a,c,e). For L' approximately greater than 30, the change in $C_{p0.1\%}$ is gradual, with a tendency to level around negative values from −0.1 to −0.2. For $C_{p99.9\%}$ near the outer edge of the horizontal step faces, the data trend is masked by the relative influence of d_c/h. However, a close look at limited ranges of d_c/h (as shown subsequently for larger values of Re and d_c/h) indicates that the overall trend

of $C_{p99.9\%}$ is similar to that previously shown for C'_p, including an increase in C_p up to the vicinity of the point of inception, followed by its decrease downstream of that location, steeply in an initial reach, and mildly further downstream (i.e., $L' > 30$). Similar behavior was found for the other corresponding extreme pressure coefficients, i.e., $C_{p5.0\%}$ and $C_{p1.0\%}$, for the vertical faces, and $C_{p95.0\%}$ and $C_{p99.0\%}$, for the horizontal faces (not shown herein).

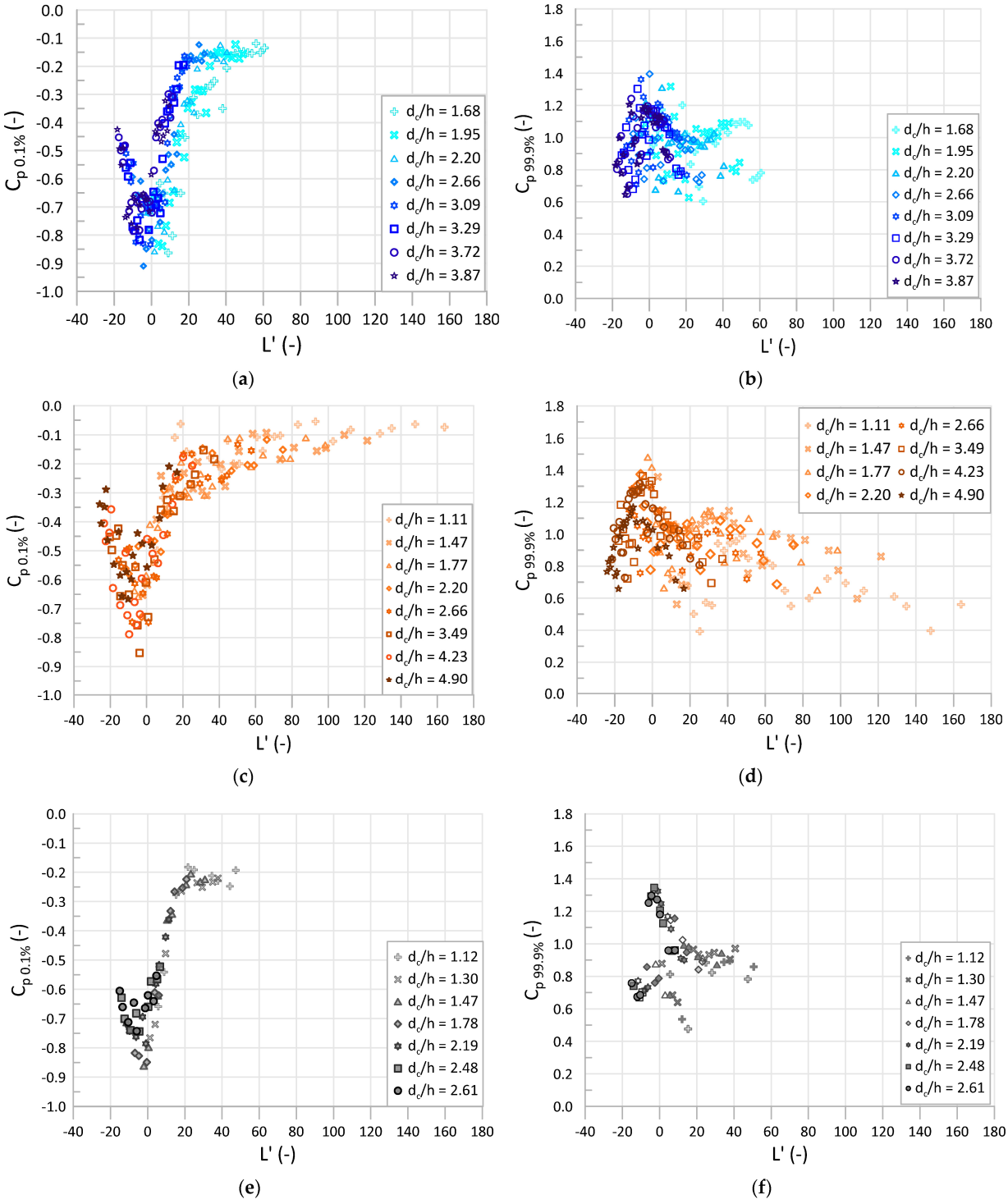

Figure 9. Streamwise development of the 0.1% (left) and 99.9% (right) extreme pressure coefficients, at the LOH I (blue color), LOH II (brown color), and LAHE (grey color) stepped chutes: (**a**,**c**,**e**) vertical face of the step, near the outer edge; (**b**,**d**,**f**) horizontal face of the step, near the outer edge.

Figure 10 shows the development of $C_{p0.1\%}$, $C_{p1.0\%}$, and $C_{p5.0\%}$ near the outer edge of the vertical face of the steps along the stepped chutes. In Figure 10a,c,e, complete data sets were used, whereas in Figure 11b,d,f, only data for $Re \geq 2 \times 10^5$ and $d_c/h \geq 1.78$ were included (Tables 1 and 2). The empirical formulae proposed by [22,27] for $C_{p0.1\%}$, are also plotted, along with a new model developed from the present data set (Equation (7), for $-25 \leq L' \leq 50$, along with Table 3). Again, dashed lines were used herein when extending the range of application of the models by [22,27], or for the model developed within the scope of this study. Overall, the development of both $C_{p5.0\%}$ and $C_{p1.0\%}$ is similar to that obtained for $C_{p0.1\%}$. The model proposed by [27] is able to identify the increasing and decreasing trends of $C_{p0.1\%}$, $C_{p1.0\%}$, or $C_{p5.0\%}$, even though the respective minima are obtained shortly downstream of that derived from Equation (7). The $C_{p0.1\%}$ model presented in [22] for $L' \geq 0$ fits the data well in a reach downstream of the point of inception (i.e., $L' \leq 15$). Further downstream, larger negative values are predicted from the [22] model, in comparison to the data acquired in the present study.

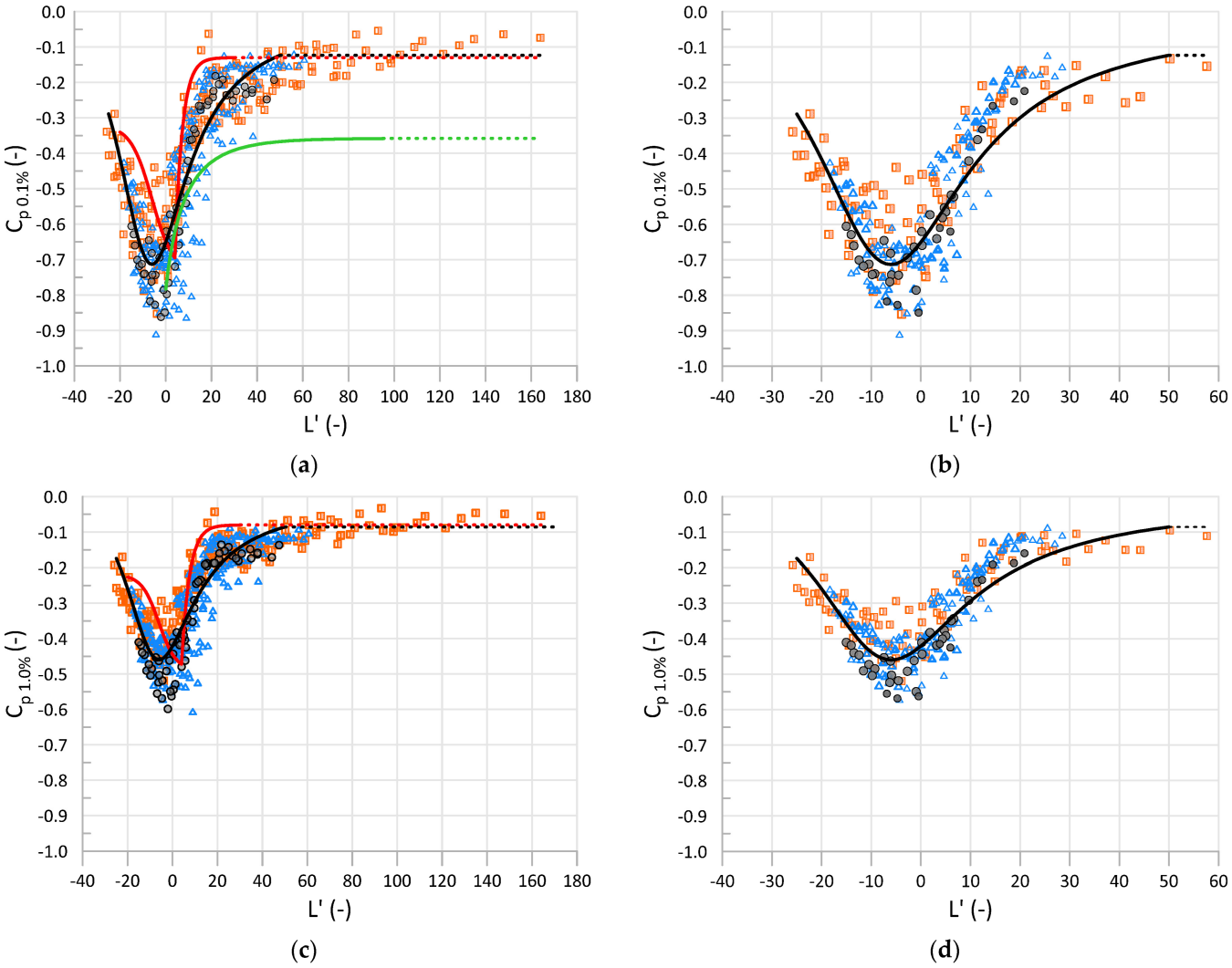

Figure 10. *Cont.*

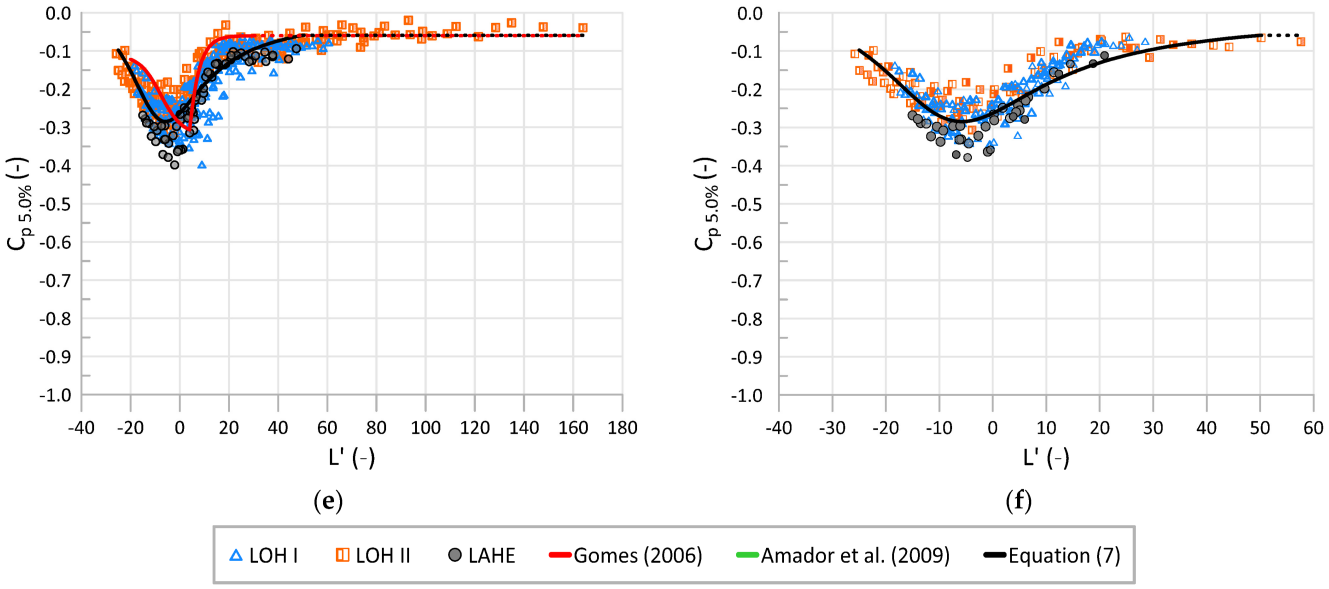

Figure 10. Streamwise development of the 0.1%, 1.0% and 5.0% extreme pressure coefficients on the vertical face of the step, near the outer edge, at the LOH I (blue color), LOH II (brown color), and LAHE (grey color) stepped chutes, for: (**a**,**c**,**e**) complete data set; (**b**,**d**,**f**) data relative to $Re \geq 2 \times 10^5$ and $d_c/h \geq 1.78$.

The results obtained for all models considering data satisfying the condition $Re \geq 2 \times 10^5$ and $d_c/h \geq 1.78$ exhibit a similar trend, which sustains the applicability of the model for high values of d_c/h and Re (Figure 10b,d,f).

$$C_p = \frac{a + bL'}{1 + cL' + dL'^2} \quad (7)$$

The development of $C_{p95.0\%}$, $C_{p99.0\%}$, and $C_{p99.9\%}$ near the outer edge of the horizontal face of the steps along the chutes is shown in Figure 11. In Figure 11a,c,e, complete data sets were used, whereas in Figure 11b,d,f, only data for $Re \geq 2 \times 10^5$ and $d_c/h \geq 1.78$ were included (Tables 1 and 2). The empirical formulae proposed by [27] are also plotted. Overall, the development of both $C_{p95.0\%}$ and $C_{p99.0\%}$ is similar to that obtained for $C_{p99.9\%}$. The model proposed by [27] overestimates $C_{p95.0\%}$, $C_{p99.0\%}$, and $C_{p99.9\%}$ in the vicinity of the point of inception. When considering the model results for $Re \geq 2 \times 10^5$ and $d_c/h \geq 1.78$, the data scatter is considerably reduced. Near the point of inception, $0.8 \leq C_{p99.9\%} \leq 1.4$, $0.6 \leq C_{p99.0\%} \leq 1.1$ and $0.4 \leq C_{p95.0\%} \leq 0.8$. Hence, the pressure head corresponding to $C_{p99.0\%}$ generally surpasses the mean kinetic head of the flow. Further downstream, in the gradually varied flow region, the extreme pressure coefficients are dampened, due to significant air entrainment and increased flow velocity, approaching $C_{p99.9\%} \sim 0.8$, $C_{p99.0\%} \sim 0.6$, and $C_{p95.0\%} \sim 0.4$. For $0 \leq L' \leq 50$, the overall trend of the data is qualitatively well-depicted using Equation (7), with the respective constants included in Table 3. However, the data scatter is considerable, which explains the low values of R^2.

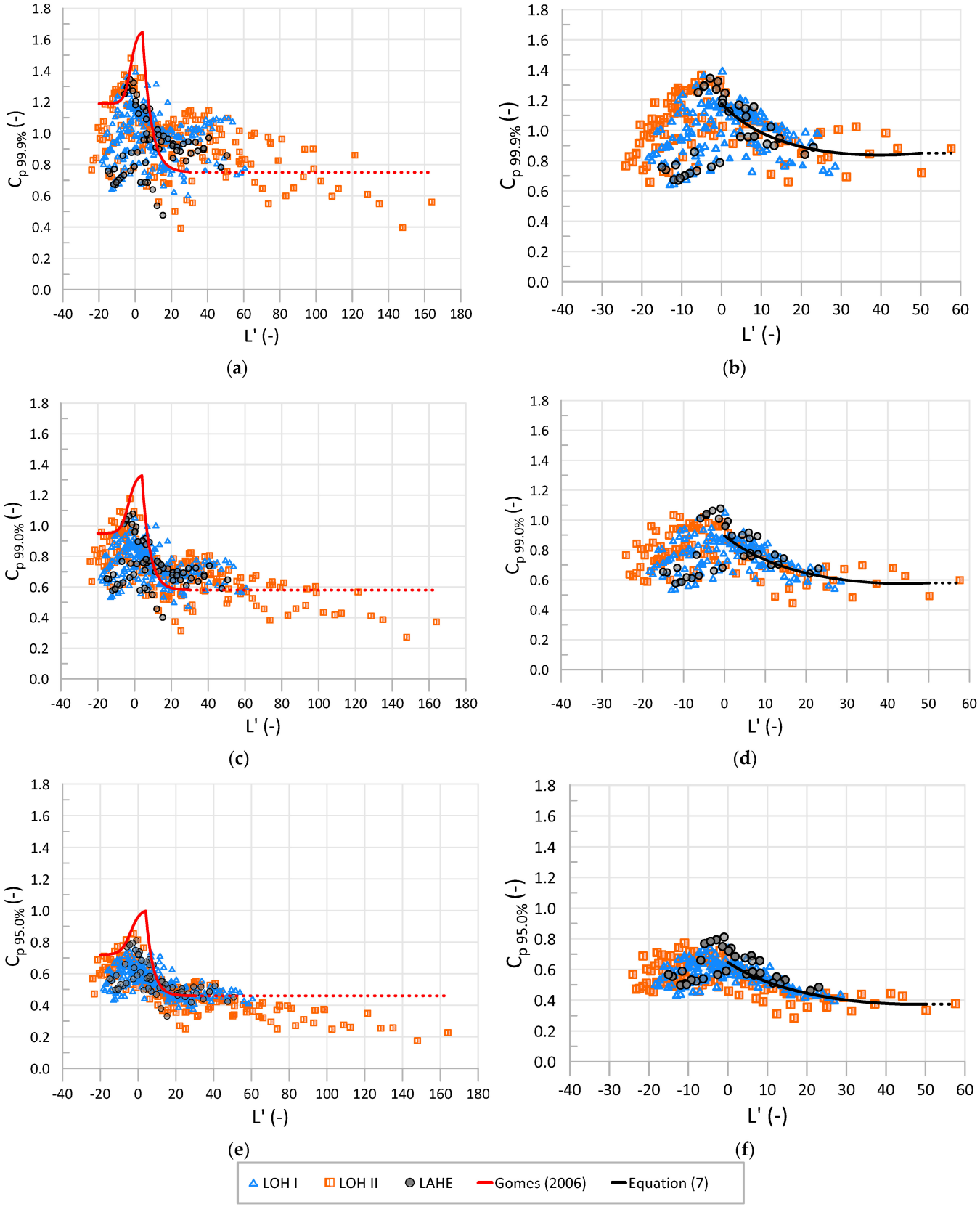

Figure 11. Streamwise development of the 99.9%, 99.0%, and 95.0% extreme pressure coefficients on the horizontal face of the step, near the outer edge, at the LOH I (blue color), LOH II (brown color), and LAHE (grey color) stepped chutes, for: (**a**,**c**,**e**) complete data set; (**b**,**d**,**f**) data relative to $Re \geq 2 \times 10^5$ and $d_c/h \geq 1.78$.

4.4. Risk of Cavitation: Application to Prototypes

The estimation of the flow conditions that may lead to cavitation on 1V:0.75H steeply sloping stepped spillways was carried out using two distinct approaches. This first one was based on the findings of [54,55], where the pressure with 0.1% probability of non-exceedance was suggested as a representative extreme negative pressure for cavitation tendency verification in macroturbulent flows, based on model–prototype comparisons.

Hence, the empirical model developed herein for predicting $C_{px\%}$ near the outer edge of the vertical step face was used to estimate the critical velocity down the chute [21,22,27,29],

$$U_{crit} = \sqrt{\frac{2g\,p_v/\gamma}{C_{px\%}}} \quad (8)$$

where p_v is the vapor pressure (p_v/γ = 0.24 m, for t = 20 °C), and U_{crit} the critical water velocity taken herein as the velocity which would virtually lead to the occurrence of vapor pressure at prototype, near the outer edge of the vertical face of the step.

Based on the complete set of data, the minimum values of $C_{p0.1\%}$ ranged between −0.45 and −0.9, whereas the application of the empirical model yielded an intermediate value of approximately −0.7, shortly upstream of the point of inception, at $L' = -6$ (Figure 10a). This value is identical to that obtained by the model of [27]; however, according to [27], the minimum value is estimated shortly downstream of the point of inception. Also, the minimum value obtained in this experimental study agrees with the conservative value proposed by [22] at the point of inception on a 1V:0.8H sloping chute ($C_{p0.1\%} = -0.9$).

The cavitation index σ can be estimated from [2,56],

$$\sigma = \frac{(p - p_v)/\gamma}{U^2/2g} \quad (9)$$

where p the pressure at the pseudo-bottom, assuming an hydrostatic pressure distribution (i.e., $p = p_{atm} + \gamma d\cos\theta$, where p_{atm} is the atmospheric pressure). Considering $U = U_{crit}$ and $d = q/U_{crit}$, the critical cavitation index based on $C_{p0.1\%}$ ($\sigma_{c\,(Cp0.1\%)}$) may be calculated from Equation (9). Similarly, predictions of the critical cavitation index based on $C_{p1.0\%}$ ($\sigma_{c\,(Cp1.0\%)}$) and $C_{p5.0\%}$ ($\sigma_{c\,(Cp5.0\%)}$) were also obtained. In Figure 12, the development of $\sigma_{c\,(Cp0.1\%)}$, $\sigma_{c\,(Cp1.0\%)}$, and $\sigma_{c\,(Cp5.0\%)}$ along 1V = 0.75H sloping stepped spillways commonly found on RCC dams is plotted for selected values of the step height and unit discharge. The results show a consistent behavior of the critical cavitation indexes along the chute, rapidly increasing upstream of the point of inception of air entrainment, reaching a peak in the upstream vicinity of that location, and decreasing downstream of such a peak, steeply in an initial reach, and more gradually further downstream. For identical L', higher values of the critical cavitation index were obtained for decreasing pressure probabilities of non-exceedance, as expected.

Also plotted in Figure 12 is the cavitation index (σ) along the chute obtained from Equation (9), where the mean water velocity and the pressure head at the pseudo-bottom at each cross section in the non-aerated region was determined from Equation (3), along with Equations (1) and (2), with $p = p_{atm} + \gamma d\cos\theta$; in the self-aerated region, Equations (4) and (5) were used for estimating the equivalent clear water depth, for $d_c/h \leq 3$ and for $d_c/h > 3$, respectively. In the chute reach where $\sigma < \sigma_{c\,(Cp0.1\%)}$, it is assumed that there is the risk of occurrence of cavitation. However, provided that the air concentration close to the pseudo-bottom (Equation (6)) is larger than a critical value, cavitation damage is not expected to occur, even if cavitation may take place [57]. Hence, a potential risk of cavitation damage may occur on the reach where $\sigma < \sigma_{c\,(Cp0.1\%)}$ and $C_b < 0.08$, as indicated in Figure 12 as gray shaded zones. Therein one can observe that for a stepped spillway with 0.6 m high steps, σ is slightly lower that $\sigma_{c\,(Cp0.1\%)}$ in the vicinity of the point of inception for $q = 15\ m^2/s$, which corresponds practically to the maximum recommended unit discharge for such a chute based on this method. The influence of the step height on the maximum unit discharge was

found to be relatively small. For larger step heights of 0.9 m or 1.2 m, the application of the model would return larger unit discharges of q ~ 17 m^2/s and q ~ 19 m^2/s, respectively. This result is judged to stem from the fact that the $C_{p0.1\%}$ model does not take into account the influence of d_c/h, which may be considerable near the point of inception. However, the model tends to predict acceptable values of $C_{p0.1\%}$ for large relative critical depths, as expected for design conditions where cavitation may occur. For example, considering the experimental data corresponding to $Re > 3 \times 10^5$ and $d_c/h \geq 1.78$, $C_{p0.1\%}$ varied between −0.79 and −0.67, and U_{crit} between 15.7 m/s and 17.3 m/s (Equation (8)). Such critical velocities would correspond to maximum (permissible) unit discharges of approximately 13 m^2/s and 17 m^2/s for h = 0.6 m. With increasing unit discharge (on the same chute), the length of the spillway reach prone to the potential risk of cavitation damage increases, as expected (Figure 12b, grey shaded zone). However, as stated in [33], the use of the unit discharge as a design recommendation seems a bit misguided without knowing the actual conditions of when and if cavitation will form.

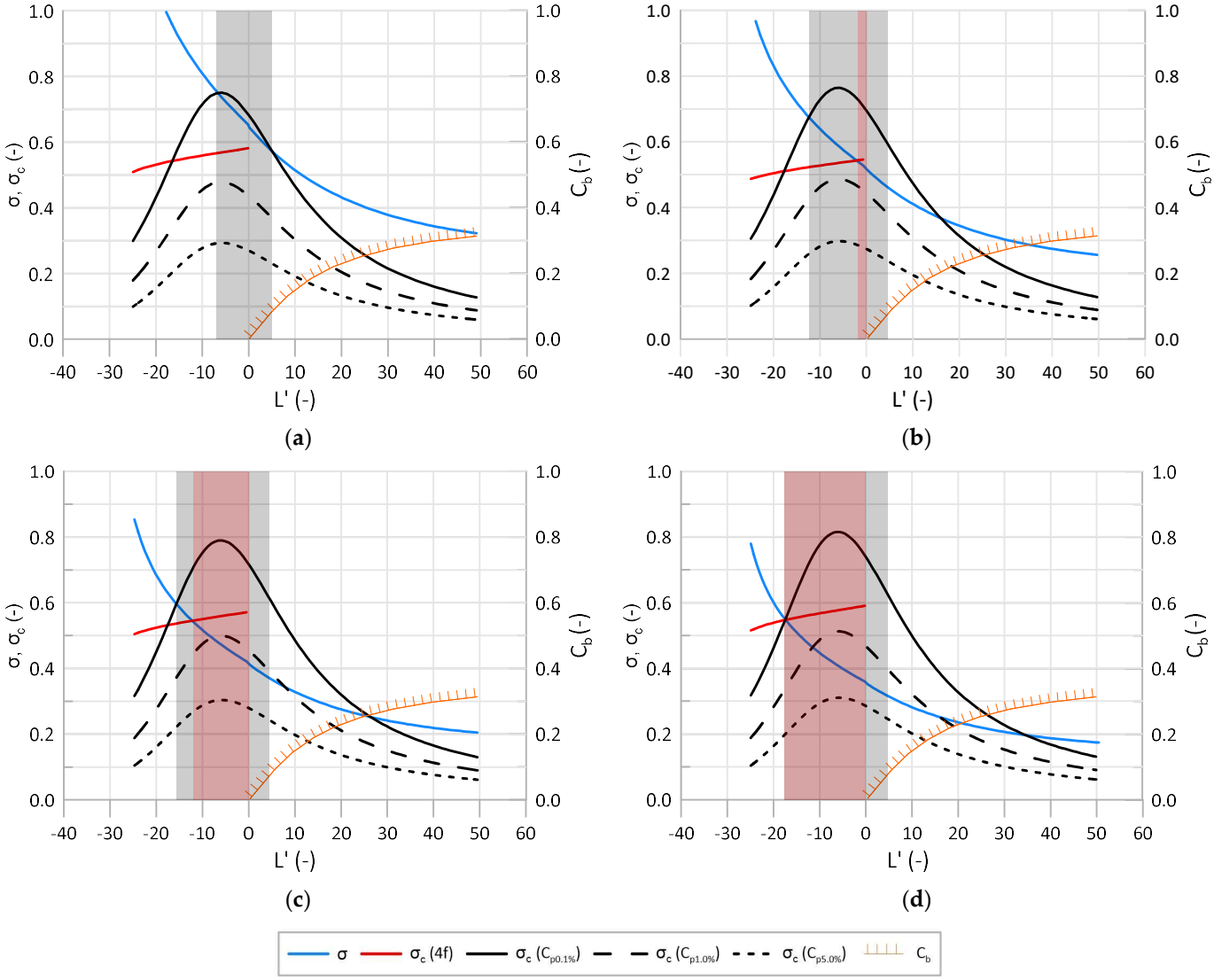

Figure 12. Cavitation index versus critical cavitation index, computed from the $C_{p5.0\%}$, $C_{p1.0\%}$, and $C_{p0.1\%}$ extreme pressure coefficients, as well as from the friction factor for the non-aerated flow region: (**a**) h = 0.6 m, q = 15 m^2/s, d_c/h = 4.74; (**b**) h = 0.6 m, q = 20 m^2/s, d_c/h = 5.74; (**c**) h = 0.9 m, q = 30 m^2/s, d_c/h = 5.01; (**d**) h = 1.2 m, q = 40 m^2/s, d_c/h = 4.55.

The second approach for estimating the flow conditions that lead to the onset of cavitation on 1V:0.75H steeply sloping stepped spillways was based on the correlation between the critical cavitation index and the friction factor proposed for uniformly distributed roughnesses in turbulent boundary layers [33,34,56] (Equation (10)). In [33], the critical cavitation index represented the point of the largest increase in the rate of cavitation activity.

The friction factor in the non-aerated flow region was estimated from Equation (11), which resulted from a reanalysis of closed conduit data for 53° sloping chutes gathered by [13], as per [2,35,51]. Even though Equation (11) was derived from closed conduit air flow, the application of this formula was found to be a good prediction of the non-aerated friction factor on a similar slope, calculated using the Von Karman's integral momentum equation [21,58].

$$\sigma_c = 4\,f \tag{10}$$

$$\frac{1}{\sqrt{f}} = 2.20 - 1.14\log\left(\frac{k}{d}\right) \tag{11}$$

The critical cavitation index estimated from Equations (10) and (11) ($\sigma_{c\,(f)}$) is also plotted in Figure 12 (for the non-aerated flow region), where the equivalent clear water depth at each cross section was determined by applying Equation (3), along with Equations (1) and (2). According to this methodology, the risk of occurrence of cavitation occurs in the chute reach for $\sigma < \sigma_{c\,(f)}$. The value of $\sigma_{c\,(f)}$ at the point of inception varies between 0.55 to 0.60, which is of the same order of magnitude as that found by [33] for the 68° steep slope using laboratory experiments in a specialized reduced ambient pressure chamber ($\sigma_c \sim 0.63$); also, it is of the same order of magnitude as that adopted by [59] for stepped spillways up to $\theta = 55°$ ($\sigma_c = 0.5$), and those obtained by [60] ($\sigma_c = 0.5$–0.7). In the latter study, the cavitation index σ was computed according to [56], based on "average hydraulics", for the limiting discharge of 15 m^2/s of [22] on $\theta = 50°$ chutes, for distinct step heights of h = 0.3 and 1.2 m. On the other hand, $\sigma_{c\,(f)}$ is smaller than $\sigma_{c\,(Cp0.1\%)}$, in the vicinity of the point of inception ($\sigma_{c\,(Cp0.1\%)} \sim 0.75$–$0.8$).

As illustrated in Figure 12a,b, cavitation is not expected to occur in the non-aerated region for 1V:75H sloping stepped spillways with 0.6 m high steps for unit discharges up to almost 20 m^2/s. More precisely, solving the equation $\sigma = \sigma_{c\,(f)}$ at the point of inception yields $q \sim 18$ m^2/s [2]. The influence of the step height on the maximum unit discharge is relatively small, where approximately 17 m^2/s and 15 m^2/s were obtained for 0.9 m and 1.2 m high steps, respectively. The relative differences between the maximum recommended unit discharge obtained from $\sigma_{c\,(Cp0.1\%)}$ in relation to those from $\sigma_{c\,(f)}$ were −16%, −2%, and 20% for 0.6, 0.9, and 1.2 high steps, respectively.

For larger unit discharges, the extension of the chute prone to the risk of cavitation damage (red shaded zone in the non-aerated flow region) may be significant, as illustrated in Figure 12, namely for h = 0.9 m and q = 30 m^2/s (Figure 12c), and h = 1.2 m and q = 40 m^2/s (Figure 12d).

In light of the results obtained herein, it is considered advisable not to adopt design unit discharges considerably larger than 15–20 m^2/s in the steeply sloping stepped spillways of large dams, provided that artificial air entrainment is not introduced in the flow (e.g., by piers or aerators). In [61–64], for example, it is shown that the use of aerators may enable the considerably increase of the maximum (permissible) unit discharge. In addition, for dam spillways of small to moderate heights, larger unit discharges may also be considered adequate, provided that $\sigma > \sigma_c$ is assured down the chute on the non-aerated flow region [27,29,65,66]. It should be noted, however, that the values that result from predicting the onset of cavitation are conservative in terms of predicting damage. The severity of damage that may be expected is related both to the intensity of cavitation and time of exposure [56,67].

5. Conclusions

Evaluating the fluctuating pressure field on the step faces, along with the conditions leading to the onset of cavitation and protection against cavitation damage, is of utmost importance for a sound design of steeply sloping stepped spillways on large dams. Limited published guidance is available for estimating the minimum ($p_{0.1\%}$) and maximum ($p_{99.9\%}$) extreme pressures near the outer edges of the vertical or horizontal faces of the steps for large relative critical depths (i.e., $d_c/h > 3$), with a considerable reach of the chute subject to non-aerated flow conditions, as commonly adopted in design practice. These circumstances encouraged a physical model study based on three relatively large-size physical models of stepped spillways, including a vast number of simultaneous instantaneous pressure measurements, along with a broad range of tested unit discharges (up to 0.5 m^2/s) and relative critical depths (up to 4.9). In addition, the comparative analysis of the development of cavitation risk on the non-aerated flow region from $p_{0.1\%}$ pressure analysis, and from the correlation of the critical cavitation index with the friction factor, undertaken in this study was, to the best of our knowledge, not available to date.

The following conclusions can be made from this study:

- The pressure development along the chutes indicates a distinct behavior of the pressure field in the non-aerated and self-aerated flow regions, generally with an overall increase of the modulus of the mean, fluctuating, and extreme pressure coefficients up to the vicinity of the point of inception of air entrainment, and a decrease further downstream. This result is in agreement with the findings of [21,22,27,28].
- Shortly downstream of the point of inception, a rapidly varied flow region is noticeable on all pressure coefficients; the downstream end of this region agrees in general with previous findings for other flow properties, such as the mean air concentration (i.e., $L' \sim 30$, as per [41,51]).
- The fluctuating and extreme pressure coefficients near the outer edge of the vertical face of the steps along the spillway are fitted by an empirical formula in function of L' for a broad range of relative critical depths, similarly to the findings of [21,22] for C'_p and $C_{p0.1\%}$, and by [27] for all related pressure coefficients.
- The empirical formula developed for $C_{p0.1\%}$, $C_{p1.0\%}$, and $C_{p5.0\%}$, based on all data near the outer edge of the vertical face of the steps, is generally valid even if only data that satisfy $Re \geq 2 \times 10^5$ and $d_c/h \geq 1.78$ are considered; on the other hand, the data scatter for the maximum extreme pressure coefficients $C_{p95.0\%}$, $C_{p99.0\%}$, and $C_{p99.9\%}$ near the outer edge of the horizontal face of the steps is considerably reduced for $Re \geq 2 \times 10^5$ and $d_c/h \geq 1.78$.
- When considering the model results near the outer edge of the horizontal face of the steps, for $Re \geq 2 \times 10^5$ and $d_c/h \geq 1.78$, $C_{p99.9\%}$ ranges between 0.8 and 1.4 near the point of inception, hence the corresponding pressure head generally surpasses the mean kinetic head of the flow. Further downstream, in the gradually varied flow region, the extreme pressure coefficients are dampened due to the significant air entrainment and increased flow velocity, approaching 0.8 ($C_{p99.9\%}$), 0.6 ($C_{p99\%}$), and 0.4 ($C_{p95\%}$).
- Based on the minimum extreme pressure coefficient analysis ($C_{p0.1\%}$) applied to prototypes, the critical cavitation index in the vicinity of the point of inception varied typically between 0.75 to 0.80, which is fairly similar to the values obtained from [21] ($\sigma_c \sim 0.8$) and larger than those predicted by [27] ($\sigma_c \sim 0.6$).
- From the correlation between the cavitation index and the friction factor, the cavitation index in the vicinity of the point of inception at prototypes varied typically between 0.55 and 0.60, hence lower than that predicted from $C_{p0.1\%}$.

In light of the results obtained in this study, maximum unit discharges of about 15–20 m^2/s are considered advisable on 53° (1V:0.75H) sloping large-stepped spillways (without artificial aeration), for step heights ranging from 0.6 to 1.2 m. For significantly larger unit discharges, a considerable reach of the spillway may be prone to the risk of

cavitation damage, depending on the intensity of cavitation, time of exposure, and concrete cavitation resistance. However, for small to moderate height dams, larger unit discharges may be considered adequate, as long as the cavitation index is greater than the critical cavitation index in the non-aerated flow region.

Author Contributions: Conceptualization, J.M. and M.G.M.; methodology, J.M., C.K.N., R.F. and M.G.M.; validation, C.K.N., R.F., M.D.P., A.V.B.C., E.D.T. and M.G.M.; formal analysis, J.M., C.K.N., R.F. and M.G.M.; investigation, C.K.N., R.F., M.D.P., A.V.B.C., E.D.T. and M.G.M.; resources, M.G.M.; data curation, C.K.N., R.F., M.D.P. and E.D.T.; writing—original draft preparation, J.M.; writing—review and editing, all authors; visualization, C.K.N., R.F., J.M. and M.G.M.; supervision, J.M. and M.G.M.; project administration, M.G.M.; funding acquisition, M.G.M. and A.V.B.C. All authors have read and agreed to the published version of the manuscript.

Funding: The experimental research was funded by the Institute of Hydraulic Research (IPH-UFRGS, Brazil) and FURNAS Centrais Elétricas (Brazil).

Institutional Review Board Statement: Not applicable.

Informed Consent Statement: Not applicable.

Data Availability Statement: Some or all data, models, or code that support the findings of this study are available from the corresponding author upon reasonable request.

Acknowledgments: The authors wish to acknowledge the National Council for Scientific and Technological Development (CNPq, Brazil), and the Coordination for the Improvement of Higher Education Personnel (CAPES, Brazil), for their support of the experimental research, and Dona Francisca Energética S.A. (DFESA, Brazil), for information related to the Dona Francisca dam.

Conflicts of Interest: The authors declare no conflict of interest. The funders had no role in the design of the study; in the collection, analyses, or interpretation of data; in the writing of the manuscript, or in the decision to publish the results.

References

1. Chanson, H. *The Hydraulics of Stepped Chutes and Spillways*; Balkema: Lisse, The Netherlands, 2002.
2. Matos, J.; Meireles, I. Hydraulics of stepped weirs and dams spillways: Engineering challenges, labyrinths of research. In Proceedings of the 5th IAHR International Symposium on Hydraulic Structures (ISHS2014), Brisbane, Australia, 25–27 June 2014; Chanson, H., Toombes, L., Eds.;
3. Frizell, K.W.; Frizell, K.H. Guidelines for hydraulic design of stepped spillways. In *Hydraulic Laboratory Report HL-2015-06*; Bureau of Reclamation: Denver, CO, USA, 2015.
4. Guo, J.; Liu, Z.; Lu, Y. Field observation on the RCC stepped spillways with the flaring pier gate on the Dachaoshan Project. In Proceedings of the 30th IAHR Biennial Congress, Thessaloniki, Greece, 24–29 August 2003; Ganoulis, J., Prinos, P., Eds.; Volume B, pp. 473–478.
5. He, G.; Zeng, X. The integral RCC dam design characteristics and optimization of its energy dissipater in Shuidong Hydropower Station. In Proceedings of the International Symposium on RCC Dams, Santander, Spain, 2–4 October 1995; pp. 405–412.
6. Chanson, H.; Bung, D.B.; Matos, J. Stepped spillways and cascades. In *Energy Dissipation in Hydraulic Structures*; Chanson, H., Ed.; CRC Press: Leiden, The Netherlands, 2015.
7. Novakoski, C. Análise da macroturbulência do escoamento sobre vertedouro em degraus com aeração induzida por defletor e câmara de ar. Ph.D. Thesis, Universidade Federal do Rio Grande do Sul (UFRGS), Porto Alegre, Brazil, 2021. (In Portuguese).
8. Bollaert, E.; Lesleighter, E.; McComber, S.; Bozorgmehr, P.; Fahey, L.; Scriven, D. Rock scour in Australia: Some latest Queensland experiences. In Proceedings of the 8th International Conference on Scour and Erosion, Oxford, UK, 12–15 September 2016; Harris, J., Whitehouse, R., Moxon, S., Eds.; CRC Press: Boca Raton, FL, USA.
9. Stojnic, I.; Pfister, M.; Matos, J.; Schleiss, A.J. Effect of 30-degree sloping smooth and stepped chute approach flow on the performance of a classical stilling basin. *J. Hydr. Eng.* **2021**, *147*, 04020097. [CrossRef]
10. Chen, Q.; Dai, G.; Liu, H. Volume of fluid model for turbulence numerical simulation of stepped spillway overflow. *J. Hydr. Eng.* **2002**, *128*, 683–688. [CrossRef]
11. Takahashi, M.; Ohtsu, I. Aerated flow characteristics of skimming flow over stepped chutes. *J. Hydr. Res.* **2012**, *50*, 51–60. [CrossRef]
12. Zhang, J.M.; Chen, J.G.; Wang, Y. Experimental study on time-averaged pressure in stepped spillway. *J. Hydr. Res.* **2012**, *50*, 236–240. [CrossRef]
13. Tozzi, M.J. Caracterização/Comportamento de Escoamentos em Vertedouros com Paramento em Degraus. Ph.D. Thesis, Escola Politécnica da Universidade de São Paulo (USP), São Paulo, Brazil, 1992. (In Portuguese).

14. Mateos, C.; Elviro, V. Stepped spillway studies at CEDEX. In Proceedings of the International Workshop on Hydraulics of Stepped Spillways, Zürich, Switzerland, 22–24 March 2000; Minor, H.E., Hager, W.H., Eds.; Balkema: Rotterdam, The Netherlands, 2000; pp. 87–94.
15. Olinger, J.C. Contribuição ao Estudo da Distribuição de Pressões nos Vertedouros em Degraus. Ph.D. Thesis, Escola Politécnica da Universidade de São Paulo (USP), São Paulo, Brazil, 2001. (In Portuguese).
16. Olinger, J.C.; Brighetti, G. Distribuição de Pressões em Vertedouros em Degraus. *Rev. Bras. Recur. Hídricos* **2004**, *9*, 67–83. [CrossRef]
17. Sánchez-Juny, M. Comportamiento Hidráulico de los Aliviaderos Escalonados en Presas de Hormigón Compactado. Análisis del Campo de Presiones. Ph.D. Thesis, Universitat Politècnica de Catalunya (UPC), Barcelona, Spain, 2001. (In Spanish).
18. Sánchez-Juny, M.; Dolz, J. Experimental study of transition and skimming flows on stepped spillways in RCC dams. Qualitative analysis and pressure measurements. *J. Hydr. Res.* **2005**, *43*, 540–548. [CrossRef]
19. Sánchez-Juny, M.; Bladé, E.; Dolz, J. Pressures on a stepped spillway. *J. Hydr. Res.* **2007**, *45*, 505–511. [CrossRef]
20. Sánchez-Juny, M.; Bladé, E.; Dolz, J. Analysis of pressures on a stepped spillway. *J. Hydr. Res.* **2008**, *46*, 410–414. [CrossRef]
21. Amador, A. Comportamiento Hidráulico de los Aliviaderos Escalonados en Presas de Hormigón Compactado. Ph.D. Thesis, Universitat Politècnica de Catalunya (UPC), Barcelona, Spain, 2005. (In Spanish).
22. Amador, A.; Sánchez-Juny, M.; Dolz, J. Developing flow region and pressure fluctuations on steeply sloping stepped spillways. *J. Hydr. Eng.* **2009**, *135*, 1092–1100. [CrossRef]
23. André, S. High Velocity Aerated Flows over Stepped Chutes with Macro-Roughness Elements. Ph.D. Thesis, EPFL, Lausanne, Switzerland, 2004.
24. André, S.; Matos, J.; Boillat, J.-L.; Schleiss, A. Energy dissipation and hydrodynamic forces of aerated flow over macro-roughness linings for overtopped embankment dams. In Proceedings of the International Conference on Hydraulics of Dams and River Structures, Tehran, Iran, 26–28 April 2004; Yazdandoost, F., Attari, J., Eds.; Taylor & Francis Group: London, UK; pp. 189–196.
25. André, S.; Schleiss, A.J. Discussion of "Pressures on a stepped spillway". *J. Hydr. Res.* **2008**, *46*, 574–576. [CrossRef]
26. Sanagiotto, D. Características do Escoamento Sobre Vertedouros em Degraus de Declividade 1V:0,75H. Master's Thesis, Universidade Federal do Rio Grande do Sul (UFRGS), Porto Alegre, Brazil, 2003. (In Portuguese).
27. Gomes, J.F. Campo de Pressões: Condições de Incipiência à Cavitação em Vertedouros em Degraus com Declividade 1V:0,75H. Ph.D. Thesis, Universidade Federal do Rio Grande do Sul (UFRGS), Porto Alegre, Brazil, 2006. (In Portuguese).
28. Gomes, J.F.; Amador, A.T.; Marques, M.; Matos, J.; Sánchez-Juny, M. Hydrodynamic pressure field on steeply sloping stepped spillways. In Proceedings of the International Junior Researcher and Engineer Workshop on Hydraulic Structures (IJREWHS'06), Montemor-o-Novo, Portugal, 2–4 September 2006; Matos, J., Chanson, H., Eds.; University of Queensland: Brisbane, Australia, 2006; pp. 71–80.
29. Gomes, J.; Marques, M.; Matos, J. Predicting cavitation inception on steeply sloping stepped spillways. In Proceedings of the 32nd IAHR Congress, Venice, Italy, 1–6 July 2007.
30. Conterato, E. Escoamento Sobre Vertedouro em Degraus com Declividade 1V:0,75H: Caracterização das Pressões e Condições de Aeração. Bachelor's Thesis, Universidade Federal do Rio Grande do Sul (UFRGS), Porto Alegre, Brazil, 2011. (In Portuguese).
31. Ostad Mirza, M.J. Experimental Study on the Influence of Abrupt Slope Changes on Flow Characteristics over Stepped Spillways. Ph.D. Thesis, EPFL, Lausanne, Switzerland, 2016.
32. Canellas, A.V.B. Pressões Extremas Atuantes nas Proximidades das Quinas dos Degraus de Vertedouros. Ph.D. Thesis, Universidade Federal do Rio Grande do Sul (UFRGS), Porto Alegre, Brazil, 2020. (In Portuguese).
33. Frizell, K.W.; Renna, F.M.; Matos, J. Cavitation potential of flow on stepped spillways. *J. Hydr. Eng.* **2013**, *139*, 630–636. [CrossRef]
34. Arndt, R.E.A.; Ippen, A. Rough surface effects on cavitation inception. *J. Basic Eng.* **1968**, *90*, 249–261. [CrossRef]
35. Matos, J.; Quintela, A.; Ramos, C. Sobre a protecção contra a erosão de cavitação em descarregadores de cheias em degraus. *Recur. Hídricos* **2000**, *21*, 91–96. (In Portuguese)
36. Lopardo, R.A. Notas sobre fluctuaciones macroturbulentas de presión, medición, análisis y aplicación al resalto hidráulico. *Rev. Lat.-Am. Hidráulica* **1987**, *2*, 109–154. (In Spanish)
37. Takahashi, M.; Yasuda, Y.; Ohtsu, I. Effect of Reynolds number on characteristics of skimming flows in stepped channels. In Proceedings of the 31st IAHR Congress, Seoul, Korea, 11–16 September 2005; pp. 2880–2889.
38. Boes, R.M. Scale effects in modelling two-phase stepped spillway flow. In Proceedings of the International Workshop on Hydraulics of Stepped Spillways, Zürich, Switzerland, 22–24 March 2000; Minor, H.E., Hager, W.H., Eds.; Balkema: Rotterdam, The Netherlands; pp. 53–60.
39. Boes, R.M.; Hager, W. Two-phase flow characteristics of stepped spillways. *J. Hydr. Eng.* **2003**, *129*, 661–670. [CrossRef]
40. Pfister, M.; Chanson, H. Two-phase air-water flows: Scale effects in physical modeling. *J. Hydrodyn.* **2014**, *26*, 291–298. [CrossRef]
41. Matos, J. Hydraulic design of stepped spillways over RCC dams. In Proceedings of the International Workshop on Hydraulics of Stepped Spillways, Zürich, Switzerland, 22–24 March 2000; Minor, H.E., Hager, W.H., Eds.; Balkema: Rotterdam, The Netherlands; pp. 187–194.
42. Meireles, I.; Renna, F.; Matos, J.; Bombardelli, F.A. Skimming, nonaerated flow on stepped spillways over roller compacted concrete dams. *J. Hydr. Eng.* **2012**, *138*, 870–877. [CrossRef]
43. Wood, I.R. Free surface air entrainment on spillways. In *Air Entrainment in Free-Surface Flows*; IAHR Hydraulic Structures Design Manual 4, Hydraulic Design Considerations; Balkema: Rotterdam, The Netherlands, 1991; pp. 55–84.

44. Chanson, H. *Hydraulic Design of Stepped Cascades, Channels, Weirs and Spillways*; Pergamon: Oxford, UK, 1994.
45. Pfister, M.; Hager, W. Self-entrainment of air on stepped spillways. *Int. J. Multiph. Flow* **2011**, *37*, 99–107. [CrossRef]
46. Meireles, I.; Matos, J.; Frizell, K. Measuring air entrainment and flow bulking in skimming flow over steeply sloping stepped chutes. In Proceedings of the Hydraulic Measurements and Experimental Methods Conference, Lake Placid, NY, USA, 10–12 September 2007.
47. Meireles, I.; Matos, J.; Melo, J.F. Modelação teórico-experimental do escoamento deslizante sobre turbilhões em descarregadores de cheias em degraus sobre barragens de betão. In *Seminário: Barragens—Tecnologia, Segurança e Interação com a Sociedade*; Comissão Nacional Portuguesa das Grandes Barragens (CNPGB): Lisbon, Portugal, 2005. (In Portuguese)
48. Chamani, M.R.; Rajaratnam, N. Characteristics of skimming flow over stepped spillways. *J. Hydr. Eng.* **1999**, *125*, 361–368. [CrossRef]
49. Boes, R.M.; Hager, W. Hydraulic design of stepped spillways. *J. Hydr. Eng.* **2003**, *129*, 671–679. [CrossRef]
50. Matos, J.; Sánchez-Juny, M.; Quintela, A.; Dolz, J. Air entrainment and safety against cavitation damage in stepped spillways over RCC dams. In Proceedings of the International Workshop on Hydraulics of Stepped Spillways, Zürich, Switzerland, 22–24 March 2000; Minor, H.E., Hager, W.H., Eds.; Balkema: Rotterdam, The Netherlands, 2000; pp. 69–76.
51. Matos, J. Emulsionamento de ar e Dissipação de Energia do Escoamento em Descarregadores em Degraus. Ph.D. Thesis, IST, Lisbon, Portugal, 1999. (In Portuguese).
52. Meireles, I. Caracterização do Escoamento Deslizante Sobre Turbilhões e Energia Específica Residual em Descarregadores de Cheias em Degraus. Master's Thesis, IST, Lisbon, Portugal, 2004. (In Portuguese).
53. Renna, F. Caratterizzazione Fenomenologica del Moto di un Fluido Bifasico Lungo Scaricatori a Gradini. Ph.D. Thesis, Politecnico di Bari, Cosenza, Italy, 2004. (In Italian).
54. Lopardo, R.A.; De Lio, J.C.; Vernet, G.F. Physical modelling on cavitation tendency for macroturbulence of hydraulic jump. In Proceedings of the International Conference on the Hydraulic Modelling of Civil Engineering Structure, British Hydromechanics Research Association, Coventry, UK, 22–24 September 1982; Stephenson, H.S., Stapleton, C.A., Eds.; pp. 109–121.
55. Lopardo, R.A.; Lopardo, M.C. Model-prototype correlation of pressure fluctuations on baffle blocks. In Proceedings of the 38th IAHR World Congress, Panama City, Panama, 1–6 September 2019. [CrossRef]
56. Falvey, H.T. *Cavitation in Chutes and Spillways*; Technical Report 42; Bureau of Reclamation: Denver, CO, USA, 1990.
57. Peterka, A.J. The effect of entrained air on cavitation pitting. In Proceedings of the Joint Meeting of the IAHR/ASCE, Minneapolis, MN, USA, 1–4 September 1953; pp. 507–518.
58. Amador, A.; Sánchez-Juny, M.; Dolz, J. Characterization of the nonaerated flow region in a stepped spillway by PIV. *J. Fluids Eng.* **2006**, *128*, 1266–1273. [CrossRef]
59. Boes, R.M. Guidelines on the design and hydraulic characteristics of stepped spillways. In Proceedings of the 24th ICOLD Congress on Large Dams, Kyoto, Japan, 6–8 June 2012; pp. 203–220.
60. Pfister, M.; Boes, R.M. Discussion of "Skimming, nonaerated flow on stepped spillways over roller compacted concrete dams". *J. Hydr. Eng.* **2014**, *140*, 07014012–1-2. [CrossRef]
61. Pfister, M.; Hager, W.; Minor, H.-E. Bottom aeration of stepped spillways. *J. Hydr. Eng.* **2006**, *132*, 850–853. [CrossRef]
62. Schiess-Zamora, A.; Pfister, M.; Hager, W.; Minor, H.-E. Hydraulic performance of step aerator. *J. Hydr. Eng.* **2008**, *134*, 127–134. [CrossRef]
63. Terrier, S. Hydraulic Performance of Stepped Spillway Aerators and Related Downstream Flow Features. Ph.D. Thesis, EPFL, Lausanne, Switzerland, 2016.
64. Terrier, S.; Pfister, M.; Schleiss, A.J. Performance and design of a stepped spillway aerator. *Water* **2022**, *14*, 153. [CrossRef]
65. Chanson, H. Discussion of "Cavitation potential of flow on stepped spillways". *J. Hydr. Eng.* **2015**, *141*, 07014025. [CrossRef]
66. Frizell, K.W.; Renna, F.M.; Matos, J. Closure to "Cavitation potential of flow on stepped spillways". *J. Hydr. Eng.* **2015**, *141*, 07015009. [CrossRef]
67. Frizell, K.; Mefford, B. Designing spillways to prevent cavitation damage. *Concr. Int.* **1991**, *13*, 58–64.